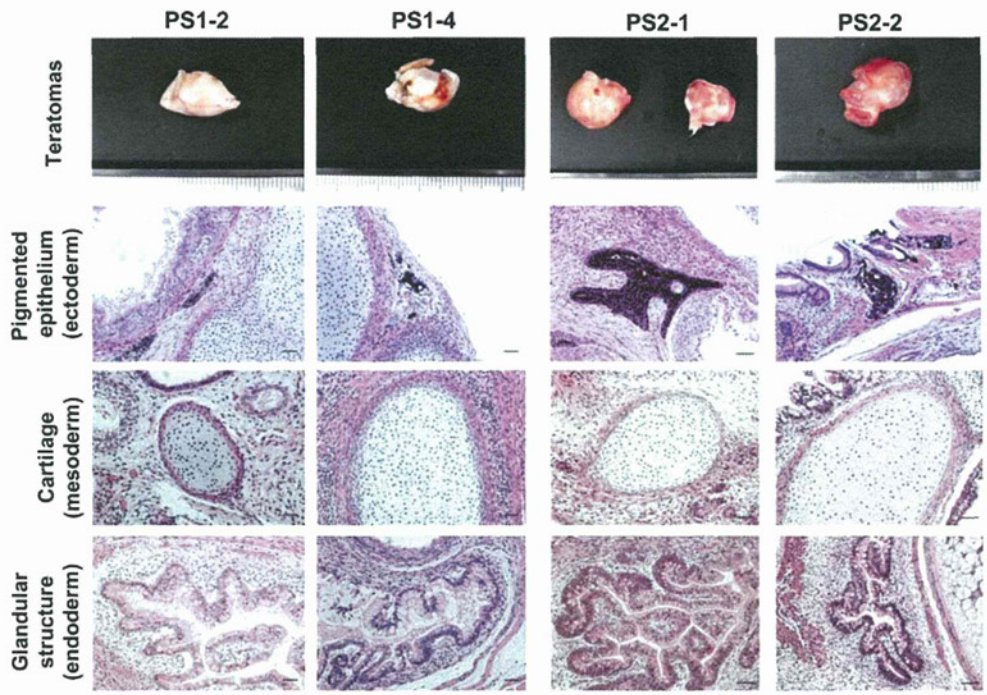

Figure 2. Teratomas derived from SCID mice injected with PS1 and PS2 iPSCs. Gross morphology, hematoxylin and eosin stained representative teratoma generated from PS 1 (PS1-2 iPSC and PS1-4 iPSC) and PS2-1 iPSC (PS2-1 iPSC and PS2-2 iPSC). Both iPSC shows tissues representing all three embryonic germ layers, including pigmented epithelium (ectoderm), cartilage (mesoderm) and glandular structure (endoderm). Bar = 50 μm.

(NICD) from both PS1-4 and PS2-2 iPSCs-derived neurons exposed to Compound E was inhibited in a dose-dependent manner. Although high dose (100 μM) of Compound W seemed to decrease NICD production in PS1-4, both neurons exposed to Compound W showed that NICD was mostly maintained (Fig. 5C). Taken together, these data indicate that both PS1 and PS2 iPSC-derived neurons respond to drug treatment in an expected manner and might be useful for drug screening in AD.

DISCUSSION

To the best of our knowledge, this study is the first to demonstrate a model of FAD using the iPSC technology. Using human neurons carrying a *PS1* mutation and a *PS2* mutation, we observed an elevation of the ratio of Aβ42 to Aβ40, a hallmark feature of FAD with presenilin mutations, in neurons derived from two clones of PS1 and PS2 iPSCs, when compared with non-AD controls (201B7, PD01-25 and 26) (Fig. 4). Although an increase in Aβ42 levels as a result of the A246E mutation in *PS1* and N141I mutation in *PS2* has been reported in patient-derived fibroblasts (11), the present study provided the first evidence of increased Aβ42 secretion by living human neurons derived from AD patients, thereby directly supporting the amyloid cascade hypothesis. To test the possibility of using the iPSC technology for drug screening, we checked the pharmacological responses to a known γ-secretase inhibitor and modulator (Fig. 5A and B). Results showed that Aβ secretion by adding agents against γ-secretase were inhibited or modulated as expected. Moreover, the Notch signaling pathway reacted with proteolytic cleavage in the presence of γ-secretase inhibitors (Fig. 5C). Recent studies have revealed that γ secretase activity is influenced in a complex manner by several cellular factors, including rafts, trafficking, expression levels of CD147, numb and gamma-secretase activating protein (1,2,29–31). We therefore propose that living human neurons from patients, i.e. FAD-iPSC-derived neurons, are very suitable material for drug development and validation of new drugs.

Previous studies on patient-specific iPSC models have mostly been limited to genetic congenital disorders (19,20,22,24,32–35). Congenital disorders may be suitable for modeling disease-specific phenotypes in the iPSC technology, because differentiated cells generated from iPSC could represent the developmental stages of disease (36). However, modeling familial PD using iPSC that carry the p.G2019S mutation in the Leucine-Rich Repeat Kinase-2 (LRRK2) gene has been reported recently (23). DA neurons derived from G2019S-iPSCs were vulnerable to exposure to stress agents, such as hydrogen peroxide, MG-132 and 6-hydroxydopamine. Now we also demonstrate the possibility of modeling the most common aging-related neurodegenerative disorder, AD, by recapitulating the key pathological mechanism (Fig. 4). Many insights into the molecular pathogenesis in neurodegenerative diseases have come from investigating post-mortem brain tissues or transgenic animals, due to the difficulty of invasive access to the living human central nervous system. With disease modeling using the iPSC technology, these new tools will make it possible to analyze living disease-specific

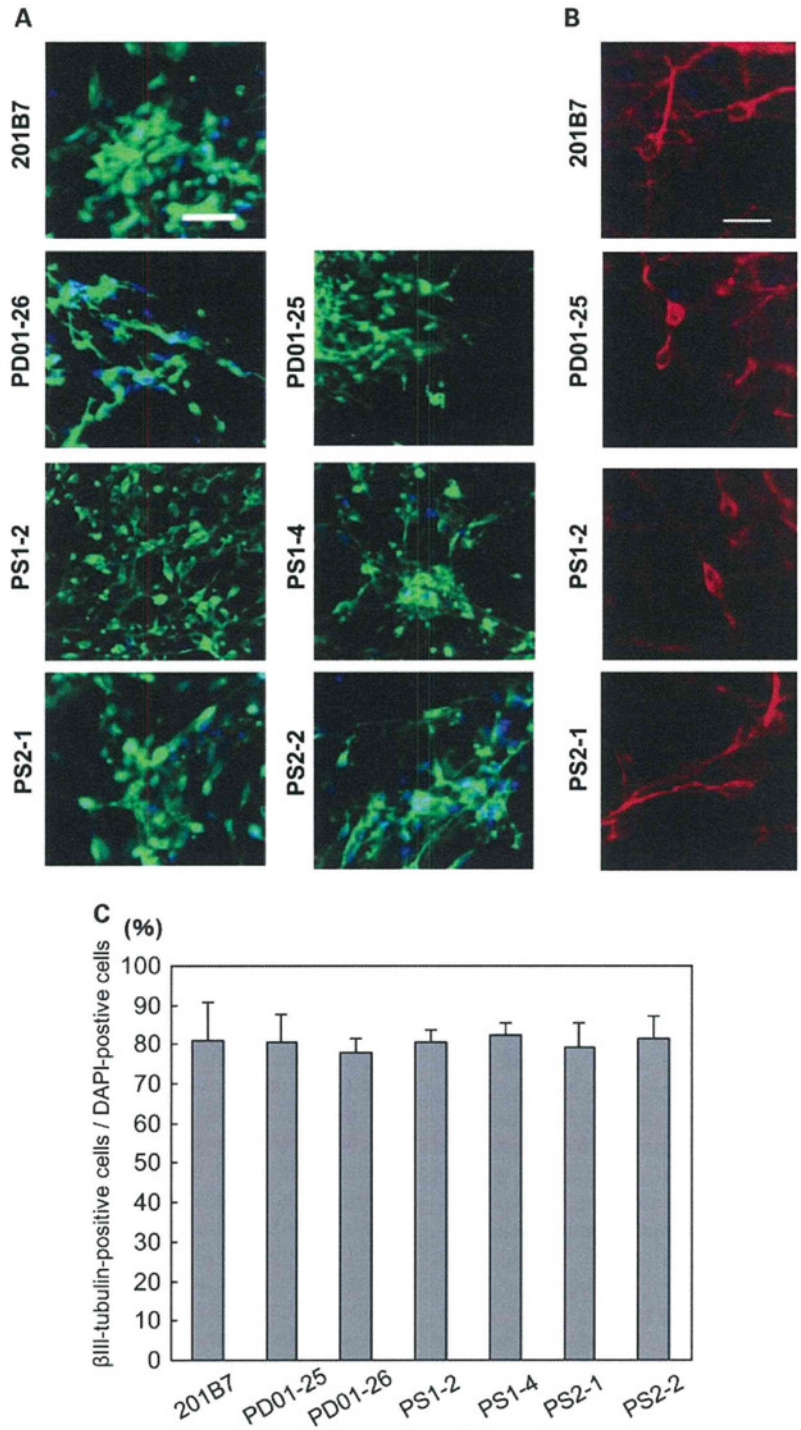

Figure 3. Differentiation of PS1 and PS2 iPSC into neurons. (**A** and **B**) Neural differentiation of control iPSC (201B7, PD01-25 and PD01-26), PS1 iPSC (PS1-2 iPSC and PS1-4 iPSC) and PS2 iPSC (PS2-1 iPSC and PS2-2 iPSC). Representative pictures of immunocytochemistry for βIII-tubulin (A) and MAP-2 (B) after neural differentiation. Bar = 40 μm (A) and 20 μm (B). (**C**) Graphs indicate the percentage of βIII-tubulin-positive cells relative to cells with DAPI-staining nuclei. Error bars indicate the SD ($n = 3$).

neurons *in vitro*. Moreover, we could graft disease-specific neurons derived from iPSCs into the brain of immunodeficient animals and we could investigate the time-dependent pathological changes *in vivo* in future studies.

FAD iPSCs could be a potential strategy for drug discovery against AD as described here; however, several limitations must be addressed in future studies. First, a high-yield of differentiated neurons from human iPSCs requires multistep

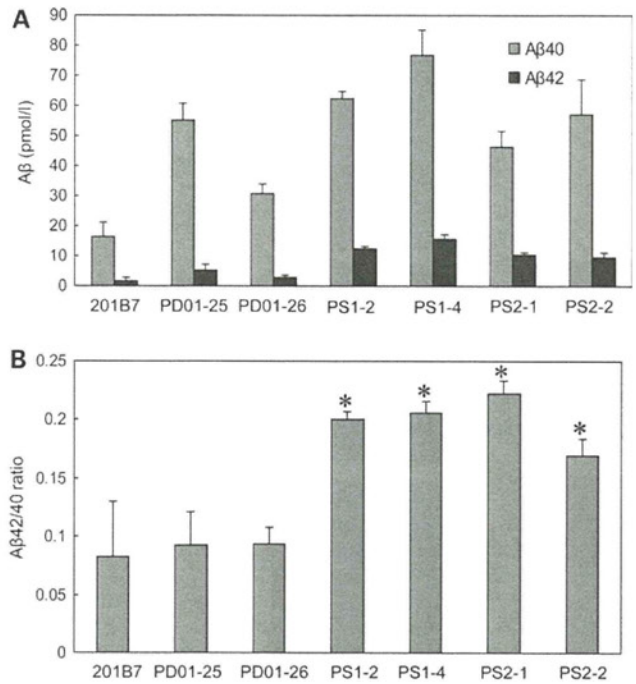

Figure 4. Characterization of Aβ secretion in PS1 and PS2 iPSC-derived neurons. (**A**) The amount of Aβ40 and Aβ42 secreted from control iPSC-derived neurons, PS1 iPSC (PS1-2 iPSC and PS1-4 iPSC) and PS2 iPSC (PS2-1 iPSC and PS2-2 iPSC)-derived neurons. (**B**) The ratio of Aβ42/Aβ40 from control iPSC-derived neurons, PS1 iPSC-derived neurons and PS2 iPSC-derived neurons. Note, the ratio of Aβ42/Aβ40 in both PS1 iPSC-derived neurons and PS2 iPSC-derived neurons was significantly higher than that of control iPSC-derived neurons. Significant differences among groups were examined by Student's *t*-test versus the ratio of 201B7 iPSC-derived neurons ($^*P < 0.05$).

procedures and prolonged culture. Furthermore, heterogeneity of differentiated neuronal cell types depending on clonal variability and culture conditions is inevitable using current differentiation methods. Clonal variation in their characters, including differentiation efficiency and tumor formation, has been a problem that needed to be solved thus far (26,37,38). Development of reliable protocols for more rapid neuronal differentiation with minimal clonal variation will be necessary, if drug discovery using iPSCs is to be fruitful. Secondly, another defining pathology in AD is an accumulation of hyperphosphorylated tau forming paired helical filaments. Growing evidence reveals that toxic Aβ directly induces tau hyperphosphorylation and accumulation, leading to neurodegeneration processes in affected neurons in AD (39,40). Pathological observations reveal that tau aggregates, but not amyloid deposits, actually correlate with dementia severity and extent of neuronal loss (41,42). Therefore, whether FAD iPSC-derived neurons exhibit accumulation of phosphorylated tau during extended culture periods should be addressed, and future studies must also focus on the biochemical dynamics of tau protein in iPSC-derived neurons treated with exogenous Aβ. Thirdly, the pathological mechanism of late-onset AD, sporadic AD and AD harboring the apoE4 allele remains unclear. Recent studies propose that impaired clearance of Aβ may cause late-onset AD through interactions with ApoE4, rather than increased Aβ production (43,44). Late-onset AD is more common and accounts for 90% of people suffering with Alzheimer's disease. To establish therapeutic strategies targeting the common form of AD, neurons derived from patient-specific iPSCs should be applied to investigations into the mechanisms underlying Aβ clearance.

Recently, a number of clinical trials of drugs targeting the pathogenesis of AD have reportedly failed in succession. Although future advances in iPSC methods are necessary for the pharmacological development and clinical application of iPSCs in neurodegeneration, we hope that our study will contribute significantly towards the identification and validation of novel candidate drugs against one of the most common and intractable diseases, AD.

MATERIALS AND METHODS

Cell culture and iPS generation

PS1 A246E fibroblasts (AG07768) and *PS2* N141I fibroblasts (AG09908) were obtained from Coriell Cell Repository. Human fibroblasts were cultured in Dulbecco's Modified Eagle's Medium (DMEM; Gibco) containing 10% fetal bovine serum, 50 U/ml penicillin, 50 mg/ml streptomycin and 1 mM L-glutamine. PS1 iPSC and PS2 iPSC were generated using the Human iPS Cell Generation Vector Set (TAKARA). G3T-hi cells were transfected with the Human iPS Cell Generation Vector set (pDON-5 OCT3/4-SOX2, pDON-5 KLF4, pDON-5 LIN28-NANOG) and pGP Vector and pE-ampho Vector with TransIT-293. Forty-eight hours after transfection, the medium (virus-containing supernatant) was collected and filtered through a 0.45 mM pore-size cellulose acetate filter. Next, the retrovirus-containing supernatant was added to RetroNectin-coated plates for centrifugation at 32°C and 2000*g* for 2 h to facilitate attachment of the virus particles onto the RetroNectin. Following this, fibroblasts were added to the plate and retrovirally transduced. Six days after transduction, fibroblasts were harvested by trypsinization and replated at 1×10^5 cells per 100 mM dish on mitomycin C-inactivated SNL cells, and the medium was changed to hiPSC medium, which consisted of DMEM/F12 medium (Invitrogen) supplemented with 20% Knock-out Serum Replacement (Invitrogen), 1 mM L-glutamine, 1 mM non-essential amino acids, 0.1 mM β-mercaptoethanol, 50 U penicillin, 50 mg/ml streptomycin (Invitrogen) and 4 ng/ml basic fibroblast growth factor (bFGF; WAKO Pure Chemicals). The hiPSC medium was changed every other day until colonies were picked. The generated iPSCs were maintained on mitomycin C-inactivated SNL cells. The hiPSC-culture medium was changed every other day, and the cells were passaged using CTK solution every 6–7 days.

Sporadic PD patient fibroblasts were generated from dermal biopsies following informed consent under protocols approved by Keio University. Two neurologists diagnosed the patient with sporadic PD, AD was excluded. Sporadic PD-derived iPSCs were generated as reported previously (14).

Reverse transcriptase-polymerase chain reaction

Total RNA samples were isolated using RNeasy (Qiagen), according to the manufacturer's instructions. The concentration

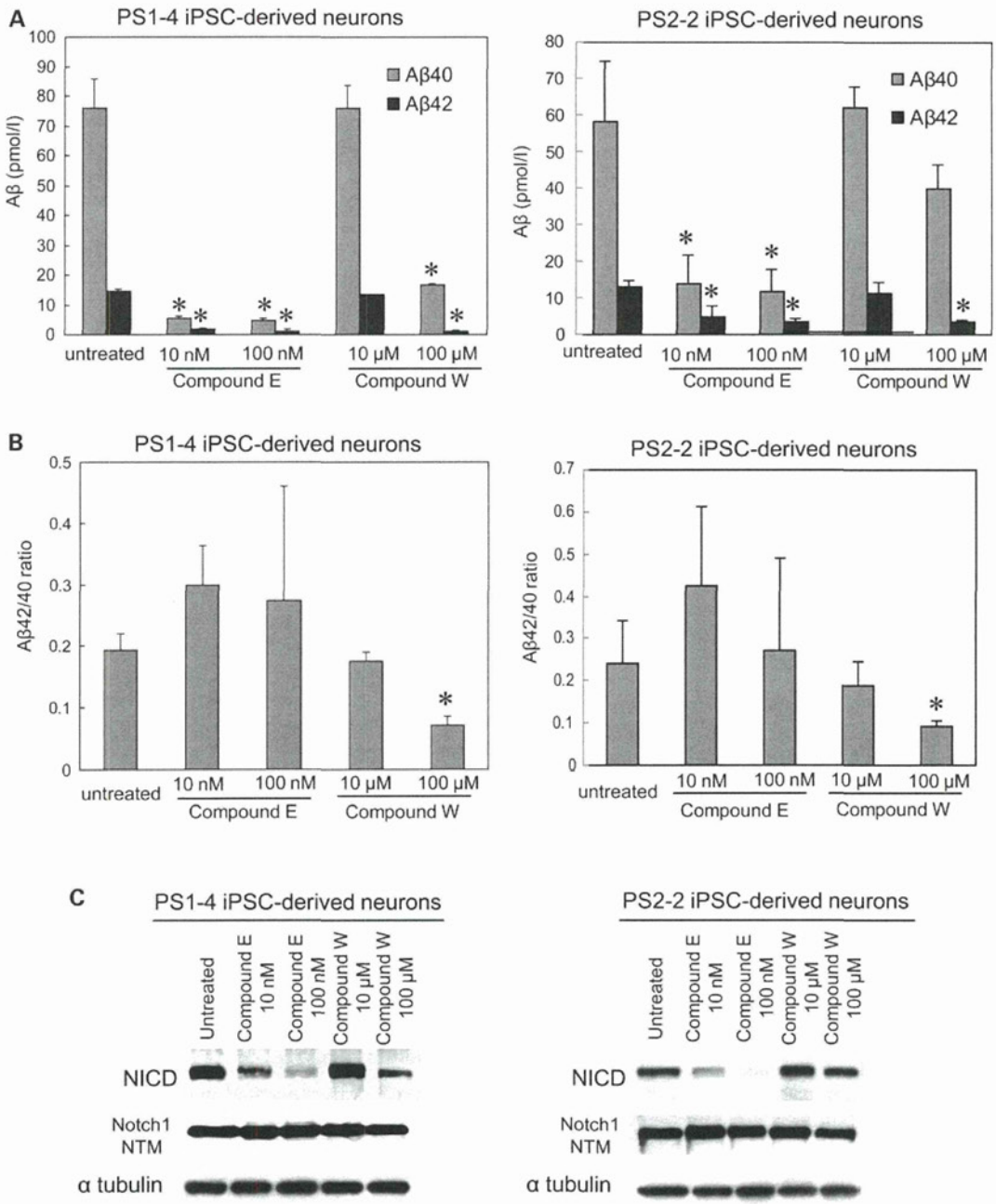

Figure 5. Pharmacological response to γ-secretase inhibitors in PS1 and PS2 iPSC-derived neurons. (**A**) The amount of Aβ40 and Aβ42 secreted from PS1-4 iPSC-derived neurons (left graph) and PS2-2 iPSC-derived neurons (right graph) treated with Compound E or W. Significant differences were examined by Student's *t*-test versus Aβ40 or Aβ42 of untreated, respectively (*$P < 0.05$). (**B**) The ratio of Aβ42/Aβ40 from PS1-4 iPSC-derived neurons (left) and PS2-2 iPSC-derived neurons (right). Significant differences were examined by Student's *t*-test versus the ratio of untreated (*$P < 0.05$). (**C**) Western blotting of S3 cleaved NICD (~110 kDa) and uncleaved Notch1 transmembrane subunit (~120 kDa) in PS1-4 iPSC-derived neurons (left) and PS2-2 iPSC-derived neurons (right) exposed to Compound E or W. α-Tubulin served as internal loading controls. Error bars in (A–D) indicate SD from three independent experiments.

and purity of the RNA was determined using the ND-1000 spectrophotometer (Nanodrop). The cDNA was synthesized using the SuperscriptIII First-Strand Synthesis System (Invitrogen). The transgene primers used in the PCR are listed in Supplementary Material, Table S2. The endogenous primers have been described previously (14).

Immunofluorescence staining of iPS and iPSC-derived differentiated neurons

Immunofluorescence staining was performed using the following primary antibodies: anti-SSEA 3 (Abcam), anti-SSEA 4 (Abcam), anti-Tra-1-60 (Millipore), anti-Tra-1-81 (Millipore),

anti-SSEA1 (Abcam), anti- MAP-2 (Chemicon) and anti-tau (HT7, Thermoscientific). 4,6-Diamidino-2-phenylindole (DAPI; Molecular Probes) was used for nuclear staining. The secondary antibodies used were: anti-rat IgG and anti-mouse IgG, and IgM conjugated with Alexa Fluor 488 or Alexa Fluor 568 (Molecular Probes).

Microarray analysis

Human genome U133 Plus 2.0 GeneChip arrays carrying 54 690 probe sets (Affymetrix) were used for microarray hybridizations to examine global gene expression. Approximately 150 ng of RNA from each sample was labeled using GeneChip 3′IVT Express (Affymetrix) according to the manufacturer's instructions. All arrays were hybridized at 45°C for 16 h and scanned using an AFX GC3000 G7 scanner. The gene expression raw data were extracted using the AFX Gene Chip Operation System. Quality control was performed on the basis of Affymetrix quality control metrics. The data were analyzed with the Gene Spring GX 11.0 (Agilent). Two normalization procedures were applied. Initially, the signal intensities with values <0.1 were assigned a value of 0.1. Then, each chip was normalized to the 50th percentile of the measurements taken from that chip. Each gene was normalized to the median of that gene in the respective controls, to enable comparisons of relative changes in gene expression levels between different conditions.

Microarray data can be found at the GEO website under accession number 'GSE28379'. (The following link has been created to allow review of record GSE28379: http://www.ncbi.nlm.nih.gov/geo/query/acc.cgi?token=zlovzkaqqwugkdg&acc=GSE28379.) The gene expression profiles of BJ fibroblasts (GSM248214) were downloaded from the NCBI Gene Expression Omnibus (GEO) database.

aCGH analysis

Genomic DNA was isolated using DNeasy (Qiagen), according to the manufacturer's instructions. DNA concentrations were measured on a Nanodrop ND-1000 spectrophotometer (Isogen). DNA quality was monitored with the Agilent 2100 Bioanalyzer (Agilent Technologies). DNA (500 ng) was labeled using the Enzo Genomic DNA Labeling kit. Hybridizations were performed on slides containing four arrays, with each array containing 622 060 *in situ* synthesized 60-mer oligonucleotides, representing 170 344 unique chromosomal locations (Agilent Technologies). Images of the arrays were acquired using a microarray scanner G2505CA (Agilent technologies) and image analysis was performed using feature extraction software version 10.7 (Agilent Technologies). The Agilent CGH-v4_107_Sep09 protocol was applied using default settings. Oligonucleotides were mapped according to the human genome build NCBI 36. The obtained data were imported into Agilent Genomic Workbench using the aberration detection method 2 (ADM-2) algorithm (10.0 threshold) for further analysis. The aCGH data have been deposited in GEO and given the series accession number GSE28450. (The following link has been created to allow review of record GSE28450: http://www.ncbi.nlm.nih.gov/geo/query/acc.cgi?token=ntsvfkqkucksgrc&acc=GSE28450.)

In vitro differentiation

Cells were harvested using CTK solutions and a cell scraper, and transferred to a Petri dish in hiPSC medium without bFGF to form embryoid bodies. After 8 days, embryoid bodies were plated onto gelatin-coated tissue culture dishes and incubated for an additional 8 days. The cells were incubated at 37°C in 5% CO_2 and the medium was replaced every other day. The cells were stained with mouse anti-α-fetoprotein IgG (R&D Systems), anti-smooth muscle actin (Sigma), anti-βIII-tubulin mouse IgG (Chemicon), together with DAPI.

Teratoma formation

hiPSCs were injected into the subcutaneous tissue of SCID mice (CREA). At 8–10 weeks post-injection, teratomas were dissected, fixed in 10% formaldehyde in PBS and embedded in paraffin.

Neural induction

Neural induction of hiPSCs cells was performed as previously described with slight modifications (Okada *et al.*, in preparation) (25,26). For terminal differentiation, induced neural cells were plated onto Matrigel-coated coverslips and cultured for 2 weeks. This was followed by the addition of Compound E, 2S-2-{[(3,5-difluorophenyl)acetyl]amino}-*N*-[(3S)-1-methyl-2-oxo-5-phenyl-2,3-dihydro-1H-1,4-benzodiazepin-3-yl]propanamide (Calbiochem) or Compound W, 3,5-Bis(4-nitrophenoxy)benzoic Acid (Tokyo Chemical Industry) for 48 h.

Quantitation of Aβ by ELISA

Conditioned media of differentiated neurons were collected after an incubation period of 48 h and subjected to β Amyloid ELISA Kits (WAKO), according to the manufacturer's instructions.

Immunoblot analysis

Cells were briefly sonicated in cold lysis buffer (50 mM Tris–HCl, pH 7.4, 150 mM NaCl, 0.5% NP-40, 0.5% sodium deoxycholate, 0.25% sodium dodecyl sulfate, 5 mM EDTA and protease inhibitor cocktail from Sigma). Total protein concentration in the supernatant was determined using a Bio-Rad protein assay kit. The proteins were then analyzed by immunoblotting as follows: protein samples were separated by reducing SDS–PAGE on a 4–20% Tris–glycine gradient gel (Invitrogen), and then transferred to a polyvinylidene difluoride membrane (Millipore). The membrane was incubated with primary antibodies and then horseradish peroxidase-conjugated secondary antibodies. Detection was performed using enhanced chemiluminescence reagents as described by the supplier (PerkinElmer Life Sciences). Primary monoclonal antibodies that were used in this study were: anti-tau (HT7, Thermoscientific), anti-NICD (Cell Signaling Technology), anti-Notch1 (D1E11) (Cell Signaling Technology) and alpha tubulin (Cell Signaling Technology).

Statistical analysis

Statistical analysis of the data was performed by Student's *t*-test using JMP 8 (SAS Institute, Inc.).

SUPPLEMENTARY MATERIAL

Supplementary Material is available at *HMG* online.

ACKNOWLEDGEMENTS

T.Y. is a research fellow of the Japan Society for the Promotion of Science. This work was supported by grants from Eisai Co. Ltd (to D.I. and N.S.) and the project for realization of regenerative medicine from the Ministry of Education, Culture, Sports, Science and Technology of Japan to H.O. We thank Mari Fujiwara (Core Instrumentation Facility, Keio University School of Medicine) for the microarray analysis and Satoko Iwasawa (Department of Preventive Medicine and Public Health, School of Medicine, Keio University) for helpful advice about statistical analysis. We also thank Dr Xu Huaxi for providing the T44 Tau pSG5 plasmid (Sanford-Burnham Medical Research Institute).

Conflict of Interest statement. None declared.

FUNDING

This work was supported by grants from Eisai Co. Ltd (to D.I. and N.S.), the Research Fellowship grant of the Japan Society for the Promotion of Science (to T.Y.), and the Project for Realization of Regenerative Medicine, and Support for Core Institutes for iPS Cell Research from the Ministry of Education, Culture, Sports, Science and Technology of Japan (to H.O.).

REFERENCES

1. Vetrivel, K.S. and Thinakaran, G. (2006) Amyloidogenic processing of beta-amyloid precursor protein in intracellular compartments. *Neurology*, **66**, S69–S73.
2. Thinakaran, G. and Koo, E.H. (2008) Amyloid precursor protein trafficking, processing, and function. *J. Biol. Chem.*, **283**, 29615–29619.
3. Hardy, J. and Selkoe, D.J. (2002) The amyloid hypothesis of Alzheimer's disease: progress and problems on the road to therapeutics. *Science*, **297**, 353–356.
4. Tanzi, R.E. and Bertram, L. (2005) Twenty years of the Alzheimer's disease amyloid hypothesis: a genetic perspective. *Cell*, **120**, 545–55.
5. Sisodia, S.S. and St George-Hyslop, P.H. (2002) gamma-Secretase, Notch, Abeta and Alzheimer's disease: where do the presenilins fit in? *Nat. Rev. Neurosci.*, **3**, 281–290.
6. Sherrington, R., Rogaev, E.I., Liang, Y., Rogaeva, E.A., Levesque, G., Ikeda, M., Chi, H., Lin, C., Li, G., Holman, K. *et al.* (1995) Cloning of a gene bearing missense mutations in early-onset familial Alzheimer's disease. *Nature*, **375**, 754–760.
7. Cruts, M., van Duijn, C.M., Backhovens, H., Van den Broeck, M., Wehnert, A., Serneels, S., Sherrington, R., Hutton, M., Hardy, J., St George-Hyslop, P.H. *et al.* (1998) Estimation of the genetic contribution of presenilin-1 and -2 mutations in a population-based study of presenile Alzheimer disease. *Hum. Mol. Genet.*, **7**, 43–51.
8. Levy-Lahad, E., Wasco, W., Poorkaj, P., Romano, D.M., Oshima, J., Pettingell, W.H., Yu, C.E., Jondro, P.D., Schmidt, S.D., Wang, K. *et al.* (1995) Candidate gene for the chromosome 1 familial Alzheimer's disease locus. *Science*, **269**, 973–977.
9. Jayadev, S., Leverenz, J.B., Steinbart, E., Stahl, J., Klunk, W., Yu, C.E. and Bird, T.D. (2010) Alzheimer's disease phenotypes and genotypes associated with mutations in presenilin 2. *Brain*, **133**, 1143–1154.
10. Borchelt, D.R., Thinakaran, G., Eckman, C.B., Lee, M.K., Davenport, F., Ratovitsky, T., Prada, C.M., Kim, G., Seekins, S., Yager, D. *et al.* (1996) Familial Alzheimer's disease-linked Presenilin 1 variants elevate Aβ1-42/1-40 ratio in vitro and in vivo. *Neuron*, **17**, 1005–1013.
11. Scheuner, D., Eckman, C., Jensen, M., Song, X., Citron, M., Suzuki, N., Bird, T.D., Hardy, J., Hutton, M., Kukull, W. *et al.* (1996) Secreted amyloid β-protein similar to that in the senile plaques of Alzheimer's disease is increased in vivo by the presenilin 1 and 2 and APP mutations linked to familial Alzheimer's disease. *Nat. Med.*, **2**, 864–870.
12. Tomita, T., Maruyama, K., Saido, T.C., Kume, H., Shinozaki, K., Tokuhiro, S., Capell, A., Walter, J., Grünberg, J., Haass, C. *et al.* (1997) The presenilin 2 mutation (N141I) linked to familial Alzheimer disease (Volga German families) increases the secretion of amyloid beta protein ending at the 42nd (or 43rd) residue. *Proc. Natl Acad. Sci. USA*, **94**, 2025–2030.
13. Oyama, F., Sawamura, N., Kobayashi, K., Morishima-Kawashima, M., Kuramochi, T., Ito, M., Tomita, T., Maruyama, K., Saido, T.C., Iwatsubo, T. *et al.* (1998) Mutant presenilin 2 transgenic mouse: effect on an age-dependent increase of amyloid beta-protein 42 in the brain. *J. Neurochem.*, **71**, 313–322.
14. Takahashi, K., Tanabe, K., Ohnuki, M., Narita, M., Ichisaka, T., Tomoda, K. and Yamanaka, S. (2007) Induction of pluripotent stem cells from adult human fibroblasts by defined factors. *Cell*, **131**, 861–872.
15. Yu, J., Vodyanik, M.A., Smuga-Otto, K., Antosiewicz-Bourget, J., Frane, J.L., Tian, S., Nie, J., Jonsdottir, G.A., Ruotti, V., Stewart, R. *et al.* (2007) Induced pluripotent stem cell lines derived from human somatic cells. *Science*, **318**, 1917–1920.
16. Dimos, J.T., Rodolfa, K.T., Niakan, K.K., Weisenthal, L.M., Mitsumoto, H., Chung, W., Croft, G.F., Saphier, G., Leibel, R., Goland, R. *et al.* (2008) Induced pluripotent stem cells generated from patients with ALS can be differentiated into motor neurons. *Science*, **321**, 1218–1221.
17. Park, I.H., Arora, N., Huo, H., Maherali, N., Ahfeldt, T., Shimamura, A., Lensch, M.W., Cowan, C., Hochedlinger, K. and Daley, G.Q. (2008) Disease-specific induced pluripotent stem cells. *Cell*, **134**, 877–886.
18. Soldner, F., Hockemeyer, D., Beard, C., Gao, Q., Bell, G.W., Cook, E.G., Hargus, G., Blak, A., Cooper, O., Mitalipova, M. *et al.* (2009) Parkinson's disease patient-derived induced pluripotent stem cells free of viral reprogramming factors. *Cell*, **136**, 964–977.
19. Ebert, A.D., Yu, J., Rose, F.F. Jr., Mattis, V.B., Lorson, C.L., Thomson, J.A. and Svendsen, C.N. (2009) Induced pluripotent stem cells from a spinal muscular atrophy patient. *Nature*, **457**, 277–280.
20. Lee, G., Papapetrou, E.P., Kim, H., Chambers, S.M., Tomishima, M.J., Fasano, C.A., Ganat, Y.M., Menon, J., Shimizu, F., Viale, A. *et al.* (2009) Modelling pathogenesis and treatment of familial dysautonomia using patient-specific iPSCs. *Nature*, **461**, 402–406.
21. Ku, S., Soragni, E., Campau, E., Thomas, E.A., Altun, G., Laurent, L.C., Loring, J.F., Napierala, M. and Gottesfeld, J.M. (2010) Friedreich's ataxia induced pluripotent stem cells model intergenerational GAA TTC triplet repeat instability. *Cell Stem Cell*, **7**, 631–637.
22. Chamberlain, S.J., Chen, P.F., Ng, K.Y., Bourgois-Rocha, F., Lemtiri-Chlieh, F., Levine, E.S. and Lalande, M. (2010) Induced pluripotent stem cell models of the genomic imprinting disorders Angelman and Prader-Willi syndromes. *Proc. Natl Acad. Sci. USA*, **107**, 17668–17673.
23. Nguyen, H.N., Byers, B., Cord, B., Shcheglovitov, A., Byrne, J., Gujar, P., Kee, K., Schüle, B., Dolmetsch, R.E., Langston, W. *et al.* (2011) LRRK2 mutant iPSC-derived DA neurons demonstrate increased susceptibility to oxidative stress. *Cell Stem Cell*, **8**, 267–280.
24. Marchetto, M.C., Carromeu, C., Acab, A., Yu, D., Yeo, G.W., Mu, Y., Chen, G., Gage, F.H. and Muotri, A.R. (2010) A model for neural development and treatment of Rett syndrome using human induced pluripotent stem cells. *Cell*, **143**, 527–539.
25. Okada, Y., Matsumoto, A., Shimazaki, T., Enoki, R., Koizumi, A., Ishii, S., Itoyama, Y., Sobue, G. and Okano, H. (2008) Spatiotemporal recapitulation of central nervous system development by murine embryonic stem cell-derived neural stem/progenitor cells. *Stem Cells*, **26**, 3086–3098.
26. Miura, K., Okada, Y., Aoi, T., Okada, A., Takahashi, K., Okita, K., Nakagawa, M., Koyanagi, M., Tanabe, K., Ohnuki, M. *et al.* (2009)

Variation in the safety of induced pluripotent stem cell lines. *Nat. Biotechnol.*, **27**, 743–745.
27. Beher, D., Wrigley, J.D., Nadin, A., Evin, G., Masters, C.L., Harrison, T., Castro, J.L. and Shearman, M.S. (2001) Pharmacological knock-down of the presenilin 1 heterodimer by a novel gamma-secretase inhibitor: implications for presenilin biology. *J. Biol. Chem.*, **276**, 45394–45402.
28. Okochi, M., Fukumori, A., Jiang, J., Itoh, N., Kimura, R., Steiner, H., Haass, C., Tagami, S. and Takeda, M. (2006) Secretion of the Notch-1 Abeta-like peptide during Notch signaling. *J. Biol. Chem.*, **281**, 7890–7898.
29. Zhou, S., Zhou, H., Walian, P.J. and Jap, B.K. (2005) CD147 is a regulatory subunit of the gamma-secretase complex in Alzheimer's disease amyloid beta-peptide production. *Proc. Natl Acad. Sci. USA*, **102**, 7499–7504.
30. He, G., Luo, W., Li, P., Remmers, C., Netzer, W.J., Hendrick, J., Bettayeb, K., Flajolet, M., Gorelick, F., Wennogle, L.P. *et al.* (2010) Gamma-secretase activating protein is a therapeutic target for Alzheimer's disease. *Nature*, **467**, 95–98.
31. Kyriazis, G.A., Wei, Z., Vandermey, M., Jo, D.G., Xin, O., Mattson, M.P. and Chan, S.L. (2008) Numb endocytic adapter proteins regulate the transport and processing of the amyloid precursor protein in an isoform-dependent manner: implications for Alzheimer disease pathogenesis. *J. Biol. Chem.*, **283**, 25492–25502.
32. Liu, G.H., Barkho, B.Z., Ruiz, S., Diep, D., Qu, J., Yang, S.L., Panopoulos, A.D., Suzuki, K., Kurian, L., Walsh, C. *et al.* (2011) Recapitulation of premature ageing with iPSCs from Hutchinson–Gilford progeria syndrome. *Nature*, **472**, 221–225.
33. Zhang, J., Lian, Q., Zhu, G., Zhou, F., Sui, L., Tan, C., Mutalif, R.A., Navasankari, R., Zhang, Y., Tse, H.F. *et al.* (2011) A human iPSC model of Hutchinson Gilford progeria reveals vascular smooth muscle and mesenchymal stem cell defects. *Cell Stem Cell*, **8**, 31–45.
34. Yazawa, M., Hsueh, B., Jia, X., Pasca, A.M., Bernstein, J.A., Hallmayer, J. and Dolmetsch, R.E. (2011) Using induced pluripotent stem cells to investigate cardiac phenotypes in Timothy syndrome. *Nature*, **471**, 230–234.
35. Carvajal-Vergara, X., Sevilla, A., D'Souza, S.L., Ang, Y.S., Schaniel, C., Lee, D.F., Yang, L., Kaplan, A.D., Adler, E.D., Rozov, R. *et al.* (2010) Patient-specific induced pluripotent stem-cell-derived models of LEOPARD syndrome. *Nature*, **465**, 808–812.
36. Mattis, V.B. and Svendsen, C.N. (2011) Induced pluripotent stem cells: a new revolution for clinical neurology? *Lancet Neurol.*, **10**, 383–394.
37. Hu, B.Y., Weick, J.P., Yu, J., Ma, L.X., Zhang, X.Q., Thomson, J.A. and Zhang, S.C. (2010) Neural differentiation of human induced pluripotent stem cells follows developmental principles but with variable potency. *Proc. Natl Acad. Sci. USA*, **107**, 4335–5340.
38. Boulting, G.L., Kiskinis, E., Croft, G.F., Amoroso, M.W., Oakley, D.H., Wainger, B.J., Williams, D.J., Kahler, D.J., Yamaki, M., Davidow, L. *et al.* (2011) A functionally characterized test set of human induced pluripotent stem cells. *Nat. Biotechnol.*, **29**, 279–286.
39. Busciglio, J., Lorenzo, A., Yeh, J. and Yankner, B.A. (1995) Beta-amyloid fibrils induce tau phosphorylation and loss of microtubule binding. *Neuron*, **14**, 879–888.
40. Jin, M., Shepardson, N., Yang, T., Chen, G., Walsh, D. and Selkoe, D.J. (2011) Soluble amyloid β-protein dimers isolated from Alzheimer cortex directly induce Tau hyperphosphorylation and neuritic degeneration. *Proc. Natl Acad. Sci. USA*, **108**, 5819–5824.
41. Bierer, L.M., Hof, P.R., Purohit, D.P., Carlin, L., Schmeidler, J., Davis, K.L. and Perl, D.P. (1995) Neocortical neurofibrillary tangles correlate with dementia severity in Alzheimer's disease. *Arch. Neurol.*, **52**, 81–88.
42. Schmitt, O., Eggers, R. and Haug, H. (1995) Quantitative investigations into the histostructural nature of the human putamen. I. Staining, cell classification and morphometry. *Ann. Anat.*, **177**, 243–250.
43. Jiang, Q., Lee, C.Y., Mandrekar, S., Wilkinson, B., Cramer, P., Zelcer, N., Mann, K., Lamb, B., Willson, T.M., Collins, J.L. *et al.* (2008) ApoE promotes the proteolytic degradation of Abeta. *Neuron*, **58**, 681–693.
44. Mawuenyega, K.G., Sigurdson, W., Ovod, V., Munsell, L., Kasten, T., Morris, J.C., Yarasheski, K.E. and Bateman, R.J. (2010) Decreased clearance of CNS beta-amyloid in Alzheimer's disease. *Science*, **330**, 1774.

EMBO
Molecular Medicine

Research Article
Stimulation of astrocyte migration favours recovery

Beneficial compaction of spinal cord lesion by migrating astrocytes through glycogen synthase kinase-3 inhibition

*Francois Renault-Mihara[1,2], Hiroyuki Katoh[2,3], Takeshi Ikegami[2,3], Akio Iwanami[2,3], Masahiko Mukaino[2], Akimasa Yasuda[2], Satoshi Nori[2], Yo Mabuchi[1], Hirobumi Tada[1], Shinsuke Shibata[1], Ken Saito[4], Masayuki Matsushita[4], Kozo Kaibuchi[5], Seiji Okada[6], Yoshiaki Toyama[2], Masaya Nakamura[2]**, Hideyuki Okano[1]**

Keywords: astrocyte; glial scar; GSK-3; migration; spinal cord injury

DOI 10.1002/emmm.201100179

Received January 11, 2011
Revised August 11, 2011
Accepted August 31, 2011

The migratory response of astrocytes is essential for restricting inflammation and preserving tissue function after spinal cord injury (SCI), but the mechanisms involved are poorly understood. Here, we observed stimulation of *in vitro* astrocyte migration by the new potent glycogen synthase kinase-3 (GSK-3) inhibitor Ro3303544 and investigated the effect of Ro3303544 administration for 5 days following SCI in mice. This treatment resulted in accelerated migration of reactive astrocytes to sequester inflammatory cells that spared myelinated fibres and significantly promoted functional recovery. Moreover, the decreased extent of chondroitin sulphate proteoglycans and collagen IV demonstrated that scarring was reduced in Ro3303544-treated mice. A variety of *in vitro* and *in vivo* experiments further suggested that GSK-3 inhibition stimulated astrocyte migration by decreasing adhesive activity *via* reduced surface expression of β1-integrin. Our results reveal a novel benefit of GSK-3 inhibition for SCI and suggest that the stimulation of astrocyte migration is a feasible therapeutic strategy for traumatic injury in the central nervous system.

INTRODUCTION

Spinal cord injury (SCI) currently has no satisfying cure. While the therapeutic potential of stem/progenitor cells from various sources, including induced pluripotent stem (iPS) cells (Tsuji et al, 2010), in cell replacement strategies is uncontested (Okano, 2010), numerous obstacles including their potential tumourigenicity (Miura et al, 2009) must be overcome. Alternative, potentially complementary, therapeutic strategies are thus still required.

Recently, using several conditional knock-out mice targeting STAT3 signalling in reactive astrocytes, we and others have observed that the compaction and seclusion of infiltrating inflammatory cells in the lesion centre by migrating reactive astrocytes during the sub-acute phase of SCI is associated with improved locomotor recovery (Herrmann et al, 2008; Okada et al, 2006). These findings suggest that reactive astrocyte migration may constitute a new therapeutic target for the early phase of SCI (Renault-Mihara et al, 2008).

Glycogen synthase kinase-3 (GSK3)-α and β are serine/threonine kinases originally identified as regulators of glycogen synthase. Based on their involvement in several signalling pathways (Forde & Dale, 2007), they are considered potential therapeutic targets for several diseases (Chico et al, 2009). The fibroblast-specific genetic deletion of GSK3-β is associated with

(1) Department of Physiology, Keio University School of Medicine, Tokyo, Japan
(2) Department of Orthopedic Surgery, Keio University School of Medicine, Tokyo, Japan
(3) National Hospital Organization, Murayama Medical Center, Musashi-murayama, Japan
(4) Department of Molecular and Cellular Physiology, Graduate School of Medicine, University of the Ryukyus, Nishihara, Japan
(5) Department of Cell Pharmacology, Graduate School of Medicine, Nagoya University, Nagoya, Japan
(6) Department of Research Superstar Program Stem Cell Unit, Graduate School of Medical Sciences, Kyushu University, Fukuoka, Japan
Corresponding author: Tel: +81 3 5363 3747; Fax: +81 3 3357 5445; E-mail: hidokano@a2.keio.jp
Corresponding author: Tel: +81 3 5363 3812; Fax: +81 3 3353 6597; E-mail: masa@sc.itc.keio.ac.jp

accelerated skin wound closure in mice (Kapoor et al, 2008). Furthermore, GSK-3 inhibition was reported to be beneficial for SCI, possibly by reducing apoptosis and promoting axonal growth (Cuzzocrea et al, 2006; Dill et al, 2008).

Taking advantage of a novel, potent specific inhibitor of GSK-3, Ro3303544, we investigated the effects of GSK-3 inhibition on astrocyte migration capability. The observation that sustained inhibition of GSK-3 stimulated astrocyte migration *in vitro* led us to administer Ro3303544 after contusive SCI in mice and examine the effects of this treatment *in vivo*.

RESULTS

Ro3303544 is more potent than a previously utilized GSK-3 inhibitor

Although the potency and specificity of Ro3303544 have been evaluated in kinase assays (Adachi et al, 2007), its potency was evaluated in more detail in primary cultures of hippocampal neurons, which are recognized as very sensitive to any toxicity. In the absence of Wnt-induced signalling, cytoplasmic β-catenin is constitutively phosphorylated by GSK-3 and degraded by the ubiquitin-proteasome system (Inestrosa & Arenas, 2010). Upon initiation of the Wnt signal and subsequent inhibition of GSK-3 activity, β-catenin accumulates in the cytoplasm, translocates into the nucleus and promotes the transactivation of various genes. Treatment of E17.5 hippocampal neurons with 1 μM Ro3303544 for 48 h resulted in a strong nuclear and peri-nuclear accumulation of β-catenin as expected (Fig 1A).

The potency of Ro3303544 was then compared to another GSK-3 inhibitor, SB415286 (Coghlan et al, 2000), previously used *in vivo* (Dill et al, 2008). To quantify the level of GSK-3 inhibition at various concentrations chosen according to their respective IC50s (0.6 and 78 nM for Ro3303544 and SB415286, respectively), the phosphorylation level of collapsin response mediator protein 2 (CRMP2) at Thr514, a specific site for phosphorylation by GSK-3 (Yoshimura et al, 2005), was examined in hippocampal neurons. Ro3303544 at 500 nM

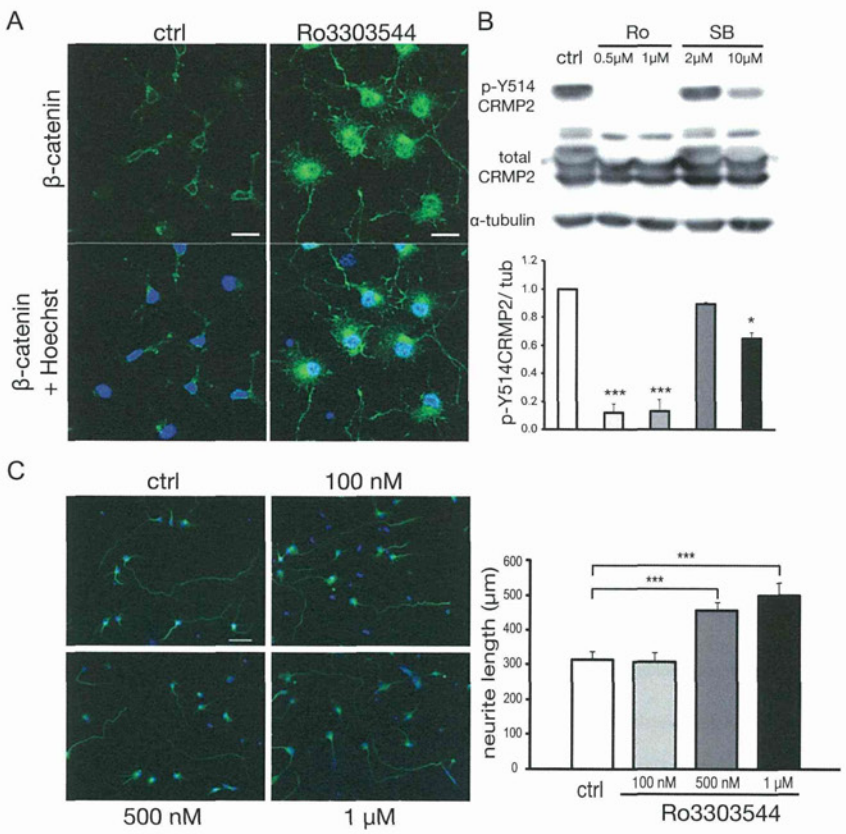

Figure 1. Ro3303544 is more potent than a previously utilized GSK-3 inhibitor.

A. Treatment of E17 rat hippocampal neurons *in vitro* with 1 μM Ro3303544 for 48 h resulted in dramatic nuclear and perinuclear accumulation of β-catenin. Scale bars: 20 μm.

B. Complete abrogation of Thr514-CRMP2 phosphorylation with Ro3303544 under the same conditions as in **A** confirmed the higher potency of Ro33034544 compared to SB415286. Data represent mean ± SEM of three independent experiments. $^{***}p < 0.001$; $^{*}p < 0.05$.

C. Treatment of E17 rat hippocampal neurons *in vitro* with Ro3303544 for 72 h significantly promoted neurite outgrowth. Green: βIII-tubulin, blue: Hoechst. Scale bar: 50 μm. Data represent mean ± SD of three independent experiments performed in triplicate. $^{***}p < 0.001$.

drastically reduced phosphorylation, in contrast to a partial effect of SB415286 at 10 μM (Fig 1B).

The treatment of E17.5 rat hippocampal neurons with Ro3303544 for 72 h *in vitro* resulted in significantly increased neurite length (mean ± SD; 58.83 ± 12.24%; Fig 1C). Together, these experiments demonstrated the high potency of Ro3303544 and its lack of toxicity at the concentrations used.

Sustained inhibition of GSK-3 stimulates the migration of astrocytes *in vitro*

Since the compaction of inflammatory cells in the lesion epicentre by reactive astrocytes during the sub-acute phase of SCI is associated with enhanced locomotor recovery (Herrmann et al, 2008; Okada et al, 2006), the stimulation of astrocyte migration is an attractive approach for the treatment of SCI during the early phase (Renault-Mihara et al, 2008). Considering that activation of the Wnt/β-catenin pathway results in the increased migration of numerous cell types in a variety of pathophysiological contexts, inhibition of GSK-3 leading to activation of β-catenin was speculated to stimulate astrocyte migration. This hypothesis was first tested *in vitro*.

Inhibition of GSK-3 by Ro3303544 was found to compromise the recolonization of a wounded area (Supporting Information, Fig S1A and Supplemental Movie 1), in agreement with the role of GSK-3 in polarization (Etienne-Manneville & Hall, 2003). Sustained GSK-3 inhibition before the migration assay was reasoned to be necessary for activating β-catenin-responsive genes. Treatment for 24 h with Ro3303544 resulted in the nuclear accumulation of β-catenin in astrocytes (Fig 2A) in a dose-dependent manner (Fig S2A and S2B). In agreement with the mitogenic effect of activated β-catenin in various cell types, these doses of Ro3303544 were observed to promote bromodeoxyuridine (BrdU) incorporation in astrocytes *in vitro* (Fig S2C).

Considering that additional treatment time would allow the completion of downstream events, we attempted to extend the Ro3303544 treatment time of astrocytes to 48 h before

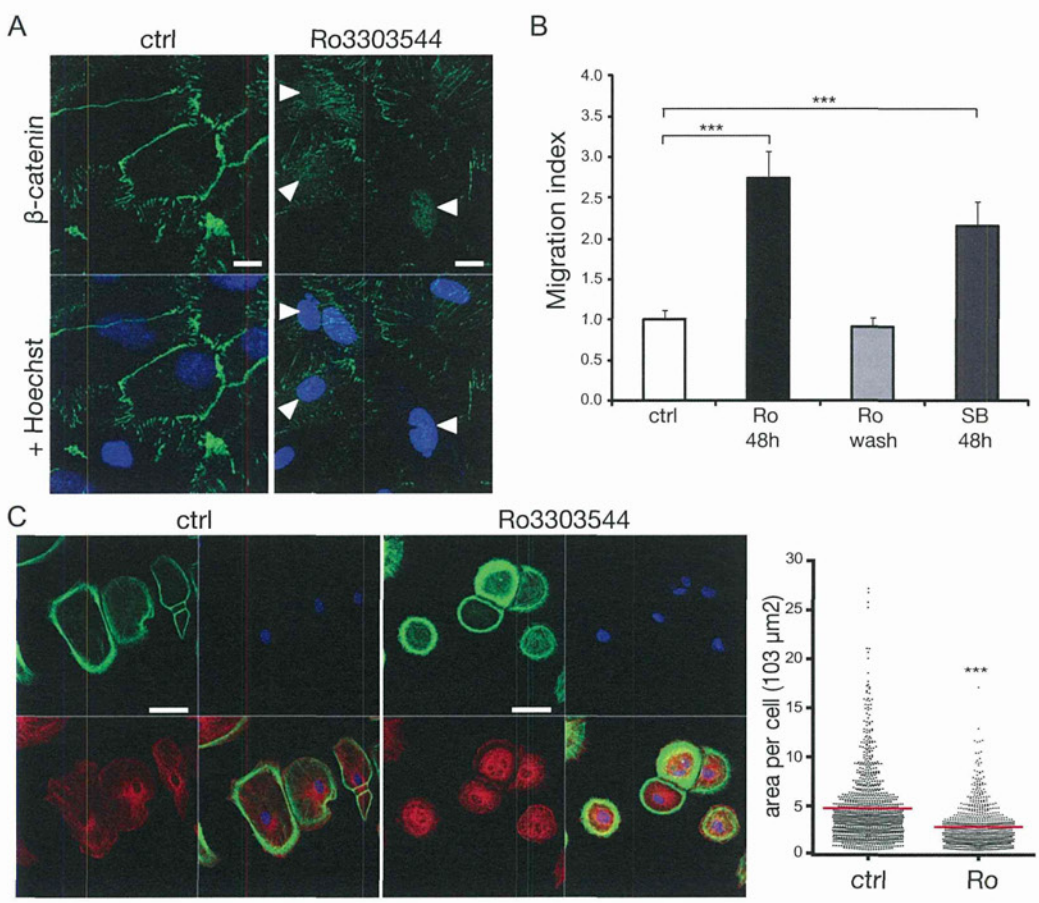

Figure 2. Sustained, but not acute, inhibition of GSK-3 by Ro3303544 stimulates the migration of astrocytes and reduces their spreading *in vitro*.

A. Treatment for 24 h with 1 μM Ro3303544 resulted in the strong nuclear accumulation of β-catenin in astrocytes (white arrowheads). Scale bar: 20 μm.

B. The sustained inhibition of GSK-3 by 48-h pretreatment with either Ro3303544 or SB415286 greatly increased astrocyte migration in a transwell assay. Washout of Ro3303544 normalized the migration index. Data represent mean ± SD of three independent experiments. $^{***}p < 0.001$.

C. Pretreatment for 48 h with Ro3303544 before seeding reduced the spreading of astrocytes onto coverslips coated with 10 μg/ml laminin. Green: F-actin labelled with phalloidin; red: α-tubulin; blue: Hoechst nuclear staining. Scale bars: 50 μm.

performing the wound scratch assay in the presence of aphidicolin, a potent antimitotic drug. However, Ro3303544 treatment sustained over 24 h was observed to disrupt the astrocytic monolayer without inducing toxicity (Fig S1B and S1C). Since intercellular contacts, mainly through adherens junctions (Dupin et al, 2009), are required for the effective recolonization of wounded astrocytic monolayers, this monolayer disruption prohibited the evaluation of 'β-catenin-activated' astrocyte migration in this assay. Therefore, a modified Boyden's chamber assay or 'transwell' assay was used, which quantifies the migration of dissociated cells through a porous membrane. Treatment of astrocytes for 48 h with 1 μM Ro3303544 before the transwell assay resulted in a 2.73 ± 0.33-fold increase in cell migration compared to control-treated astrocytes (Fig 2B and Fig S2D). A similar increase observed upon pre-treatment with 10 μM SB415286 (2.15 ± 0.30-fold increase) indicated that the stimulation of astrocyte migration was indeed due to the sustained inhibition of GSK-3, rather than to the effect of Ro3303544. The acute inhibition of GSK-3 by Ro3303544 from 30 min prior to the transwell assay until its end (15 h), a time window similar to that for the wound assay, had no significant effect on cell migration (Fig S2E) indicating that the effect of GSK-3 depended on the cell migration mode.

Dysregulated activation of the Wnt/β-catenin pathway is a common phenomenon in numerous tumours and is associated with metastatic potential (Nguyen et al, 2009). To investigate whether sustained GSK-3 inhibition promoted an irreversible, cancerous transformation of the astrocytes, Ro3303544 was removed after the initial 48 h treatment, and the astrocytes were maintained in control medium for an additional 2 days before testing their migration properties. This wash-out procedure completely normalized the migratory ability of the cells (Fig 2B), suggesting that the pro-migratory effect of sustained Ro3303544 treatment was not related to cancerous cell transformation.

Sustained inhibition of GSK-3 reduces astrocytic spreading *in vitro*

Since alterations in cell migratory properties are often associated with morphological changes, the effects of prolonged Ro3303544 treatment on astrocytic morphology were examined by staining for F-actin and α-tubulin. Ro3303544 or control solution was applied for 48 h, and then the cells were replated at a low density onto laminin-coated coverslips. After 15 h of culture, the astrocytes treated with Ro3303544 remained rounded with intense peripheral actin rings (Fig 2C), in contrast to their control counterparts, which adopted a typical astrocytic morphology. Quantitative morphometric analysis confirmed a significant reduction of the mean area per cell after treatment with Ro3303544 ($4774 \pm 3650\ \mu m^2$ and $2866 \pm 2064\ \mu m^2$, $n = 977$ and 756 analysed cells in the control and Ro3303544 group, respectively), thus demonstrating that sustained inhibition of GSK-3 reduces the spreading of astrocytes.

Inhibition of GSK-3 by Ro3303544 promotes the compaction of infiltrated inflammatory cells after spinal cord injury

Next, the *in vivo* effects of Ro3303544 after SCI were examined. To focus on the compaction of inflammatory cells by reactive astrocytes, the protocol consisted of intraperitoneal administration of Ro3303544 for only the first 5 days after thoracic contusive SCI in mice (Fig 3A). This is in contrast to a previous report in which Dill et al (2008) administered SB415286 for 3–4 weeks after SCI and reported increased axonal growth and improved functional recovery. Axonal growth is a delayed event that commences after the inflammatory reaction has subsided, while the compaction of inflammatory cells by reactive astrocytes occurs during the sub-acute phase of SCI, namely the first 2 weeks after injury in mice (Okada et al, 2006).

First, the efficiency of the protocol was evaluated. Analysis by confocal microscopy revealed that at 4 days post-injury (DPI), while phosphorylated active β-catenin (van Noort et al, 2002) was weakly expressed and localized exclusively to the cytoplasm of neurons in the spinal cords of control mice, administration of Ro3303544 resulted in β-catenin upregulation and nuclear accumulation in neurons and reactive astrocytes (Fig 3C). Immunoblotting of spinal cord lysates collected at 5 DPI quantitatively confirmed this β-catenin activation *in vivo* after administration of Ro3303544 (Fig 3B).

The effect of Ro3303544 on the compaction of inflammatory cells after SCI was then investigated. As previously observed (Okada et al, 2006), CD11b-positive inflammatory cells appeared as a diffuse infiltrate at the lesion centre of the injured spinal cord parenchyma at 7 DPI in both groups (Fig 4A) and were progressively compacted by the surrounding GFAP-positive reactive astrocytes at 14 and 42 DPI. Three-dimensional measurement of the lesion volume through the analysis of GFAP-negative areas in serial sagittal sections revealed that while the initial infiltration of inflammatory cells at 7 DPI was similar in both groups, the compaction of inflammatory cells at 14 DPI was significantly accelerated by Ro3303544 administration, consistent with the *in vitro* stimulation of astrocyte migration by Ro3303544 (Fig 4B). At 14 DPI, confocal microscopic examination of the boundary between reactive astrocytes and the lesion centre visualized through laminin confirmed the potent walling off of the lesion by reactive astrocytes in the Ro3303544-group (Fig 4C).

To examine the possibility that the increased compaction of inflammatory cells upon Ro3303544 administration *in vivo* resulted from enhanced proliferation of reactive astrocytes, BrdU incorporation experiments were performed. Mice in the control and Ro3303544 groups received daily intraperitoneal injections of BrdU for 14 days after the injury. Quantitative analysis revealed no significant difference in the number of BrdU-labelled reactive astrocytes surrounding the lesion, implying that the increased compaction of infiltrated inflammatory cells by Ro3303544 results from the migration of reactive astrocytes rather than from astrocyte proliferation (Fig 4D).

Treatment with Ro3303544 reduces the size of the lesion scar and demyelination

The lesion scar in traumatic SCI consists of a fibrous scar at the lesion core surrounded by a glial scar. Among the numerous molecules that are upregulated in CNS lesions (Sofroniew, 2009), chondroitin sulphate proteoglycans (CSPG) were exam-

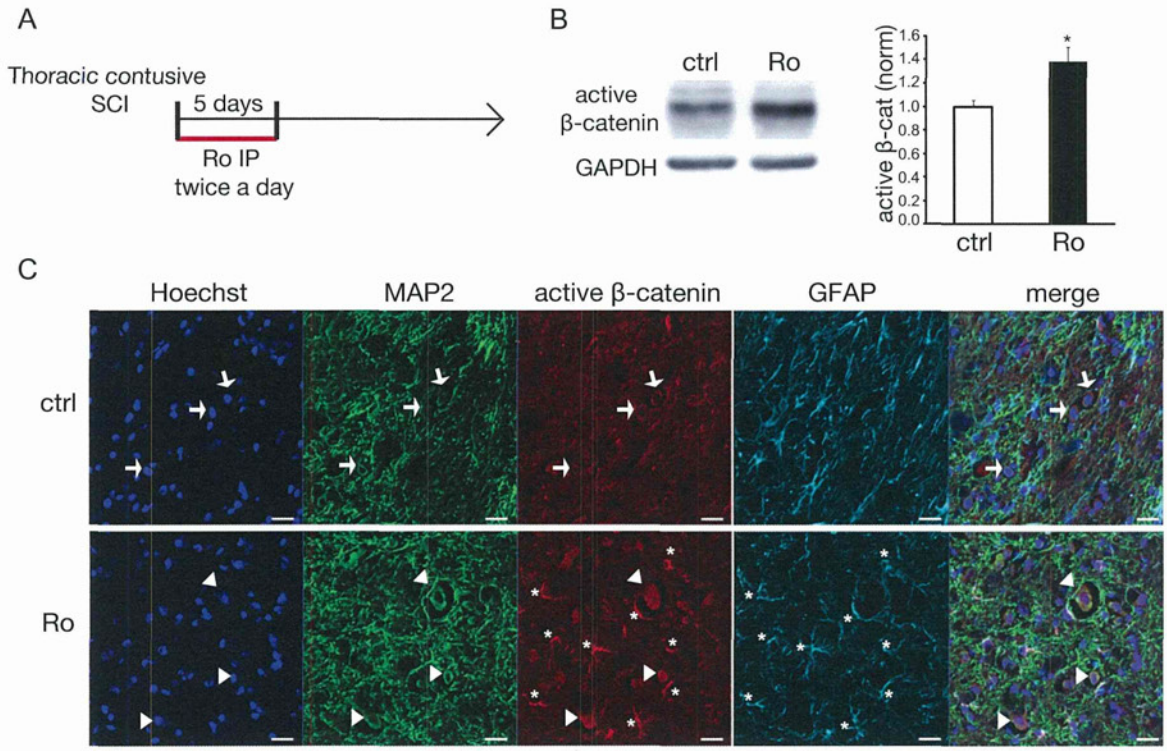

Figure 3. *In vivo* administration of Ro3303544 for the first 5 days after SCI in mice is effective.

A. Experimental design.

B. Immunoblot of spinal cord lysates at 5 DPI revealed that intraperitoneal injections of Ro3303544 potently increased the levels of a phosphorylated active form of β-catenin *in vivo*. Histogram displays the mean ± SEM of one experiment (four mice per group) ($^*p < 0.05$, Wilcoxon rank-sum test).

C. At 4 DPI, confocal analysis showed that while active β-catenin is weakly expressed and localized exclusively to the cytoplasm of neurons in the spinal cords of control mice (arrows), injections of Ro3303544 resulted in drastic upregulation and nuclear accumulation of β-catenin in neurons (arrowheads). Note that the relative upregulation of active β-catenin is even more pronounced in reactive astrocytes (asterisks).

ined first. Seminal studies have shown that CSPG staining overlapped with areas of inflammatory cell infiltration (Fitch & Silver, 1997). Quantitative analysis indicated that the area of CSPG immunoreactivity was significantly reduced in the Ro3303544 group at 14 DPI (Fig 5A) but not at 42 DPI (not shown). Considering that mice harbouring a fibroblast-specific deletion of GSK-3β exhibit accelerated wound closure as well as excessive scarring characterized by elevated collagen production (Kapoor et al, 2008), immunostaining for collagen IV, a major component of the fibrous scar (Klapka & Muller, 2006), was performed. A significant reduction of collagen IV was observed in the Ro3303544 group at 14 DPI (Fig 5B), but again not at 42 DPI (not shown). The reduction of both collagen IV- and CSPG-immunoreactive areas confirms that the stimulation of astrocyte migration by Ro3303544 is associated with reduced scar formation.

An association between compaction of inflammatory cells by migrating reactive astrocytes and a reduction in delayed neuronal damage, such as demyelination, has been previously reported (Herrmann et al, 2008; Okada et al, 2006). Accordingly, while eriochrome cyanine blue staining revealed severe demyelination, as expected, at the lesion level in the control group at 42 DPI, significantly reduced demyelination was observed in the mice treated with Ro3303544 (Fig 6A).

Administration of Ro3303544 improves motor function recovery after spinal cord injury

The recovery of motor function was then monitored over 42 days using the Basso Mouse Scale open-field score (BMS) (Basso et al, 2006). The mice in the Ro3303544 group exhibited a tendency for greater motor function recovery compared to the control group as early as 7 DPI (1.08 ± 0.97 *vs.* 1.85 ± 1.12 in the control and Ro3303544 groups, respectively). Control mice, with a mean BMS score of 2.95 ± 1.21 at 42 DPI, could not support their weight on their hind limbs. By contrast, mice in the Ro3303544 group had a mean BMS score of 5.00 ± 2.05 at 42 DPI, and many mice in this group were able to walk with forelimb–hindlimb coordination. The BMS score of the Ro3303544 group was statistically better than that of the control group (two-way repeated measures ANOVA: p-value related to an effect of the treatment = 0.0151), and Bonferroni's multiple comparisons test at each time-point demonstrated statistical significance from 21 DPI until the end of the observation period, *i.e.* 42 DPI (Fig 6B).

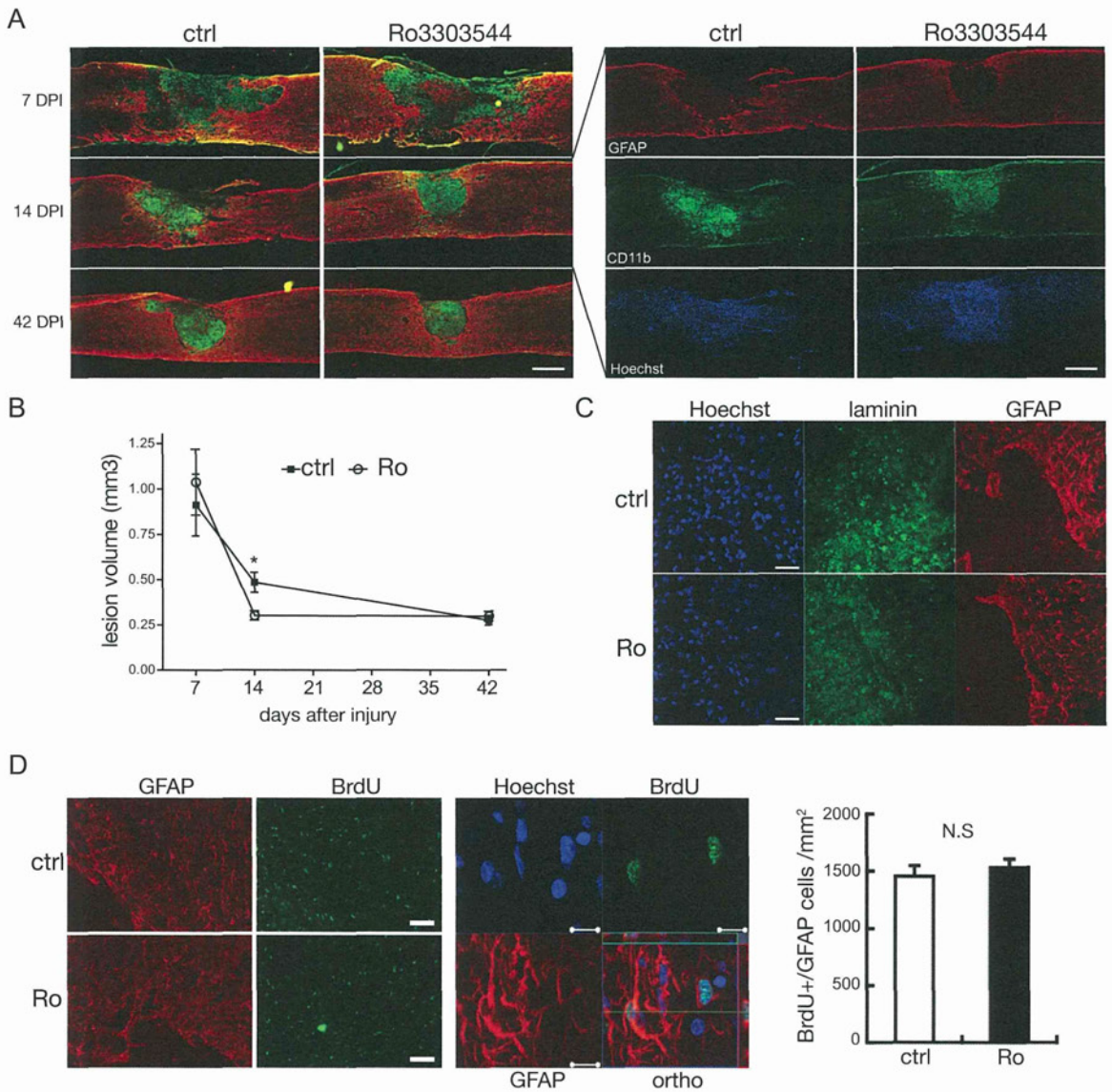

Figure 4. Administration of Ro3303544 after SCI accelerates the compaction of infiltrated inflammatory cells by stimulating reactive astrocyte migration.

A. The compaction of CD11b-positive inflammatory cells surrounded by GFAP-positive reactive astrocytes was significantly accelerated upon Ro3303544 administration. Right panels display the separate immunostaining at 14 DPI. Red: GFAP; green: CD11b; blue: Hoechst nuclear staining. Scale bars: 500 μm.

B. Lesion volume was significantly reduced at 14 DPI in the Ro3303544 group compared to control. Data represent mean ± SEM. $^{*}p = 0.011$ (Mann–Whitney test, $n = 5$ mice per group at 7 DPI and 42 DPI, $n = 12$ and 10 mice at 14 DPI in the control and Ro3303544 groups, respectively.).

C. At 14 DPI, confocal imaging of the boundary between reactive astrocytes and the lesion centre visualized through laminin revealed reactive astrocytes potently walling off the lesion in Ro3303544 group. Scale bar: 50 μm.

D. Quantification of BrdU incorporation during the first 2 weeks after the lesion did not evidence any significant difference between groups, indicating that the increased compaction did not rely on increased astrocyte proliferation *in vivo*. Confocal imaging (middle panel) illustrates BrdU/GFAP positive cells at high magnification. Histogram data represent mean ± SEM. $^{*}p < 0.05$ (Wilcoxon rank-sum test, $n = 5$ and 6 mice in the control and Ro3303544 groups, respectively). Red: GFAP; green: BrdU. Scale bars: 50 and 10 μm in the left and middle panels, respectively.

Stimulation of astrocyte migration by Ro3303544 is mediated by unknown mechanisms

What is the mechanism by which sustained Ro3303544 stimulates the migration of astrocytes? The pro-migratory effect of GSK-3β depletion in fibroblasts relies on the enhanced expression of endothelin-1 (Kapoor et al, 2008). In the case of astrocytes, the concomitant blockade of both endothelin receptors A and B by BQ-123 and BQ-788 (each 1 μM) had no effect on the pro-migratory effect of Ro3303544 (Fig S3A), indicating that different molecular mechanisms

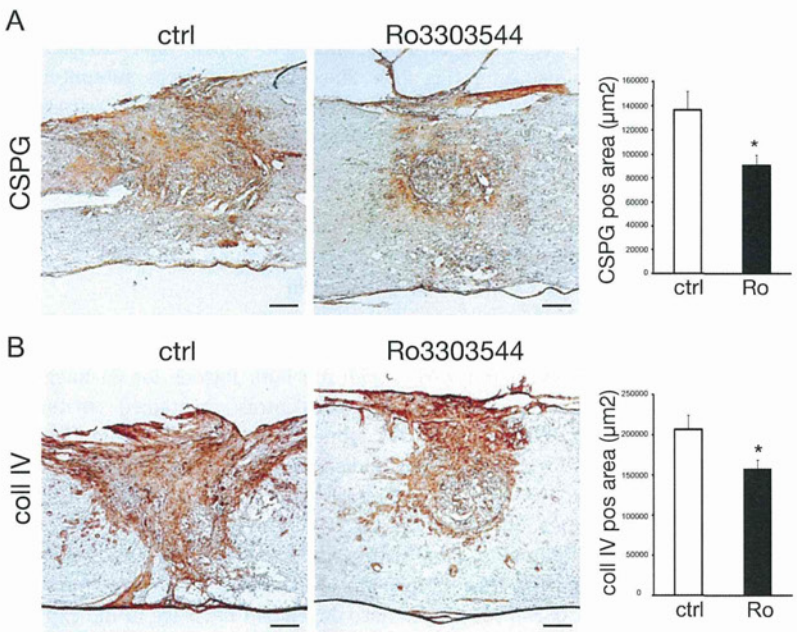

Figure 5. Treatment with Ro3303544 reduces the size of the lesion scar at 14 DPI.

A. The extent of CSPG was significantly reduced at 14 DPI in Ro3303544-treated mice.

B. The fibrous scar, assessed by collagen IV, was also significantly reduced at 14 DPI in Ro3303544-treated mice. In **A** and **B**, data represent mean ± SEM. $^{*}p < 0.05$ (unpaired *t*-test, $n = 6$ mice per group). Scale bars: 100 µm.

mediate the pro-migratory effect of GSK-3 inactivation/inhibition in astrocytes.

Next, considering that hypoxia-inducible factor 1-α (HIF-1α) promotes cell migration (Le et al, 2004) and that GSK-3 inhibition stabilizes HIF-1α (Flugel et al, 2007), Ro3303544 treatment was investigated to determine whether it could activate HIF signalling. Glioma cells were transfected with reporter constructs in which the expression of firefly luciferase was driven by hypoxia-responsive elements (HRE), and luciferase reporter assays were performed at various time-points during Ro3303544 treatment. While transfection with positive controls, *i.e.* two different gain-of-function HIF-1α mutants, enhanced HIF-dependent luminescence, treatment with Ro3303544 had no effect at any time-point (Fig S3B). This experiment thus ruled out the possible involvement of HIF signalling in the pro-migratory effect of Ro3303544. These results led to the conclusion that the stimulation of astrocyte migration by the sustained inhibition of GSK-3 could involve previously unreported mechanisms.

DNA microarray analysis suggests a global attenuation of integrin signalling in astrocytes by Ro3303544

To gain insight into the molecular mechanism underlying the pro-migratory effect of Ro3303544 treatment, DNA microarray analysis was performed using astrocytes in primary culture treated for 48 h with 1 µM Ro3303544 or control. Considering that wash-out of Ro3303544 normalized astrocyte migration (Fig 2B), this condition was also included as a control for genes that remained highly up- or downregulated after the wash-out period, which would therefore not be relevant to the Ro3303544-enhanced migration.

Figure 7A illustrates the changes in gene expression after treatment with Ro3303544 and demonstrates that the wash-out procedure partially reestablished the normal pattern. Among the 26,734 flags expressed in astrocytes, 1601 and 1638 genes were up- or downregulated more than twofold, respectively, in Ro3303544-treated astrocytes compared to control astrocytes (Fig 7B). In the wash-out *versus* vehicle groups, 1148 and 591 genes were up- or downregulated, respectively, more than twofold. Only 211 genes were upregulated and 573 genes downregulated in both the Ro3303544-treated and wash-out astrocytes compared to the control cells. Of these overlapping genes, all those for which the ratio of intensity (*i.e.* expression level) between the Ro3303544 and washout groups was below twofold were excluded.

To summarize these findings, strong variations were first observed in molecules belonging to the Wnt/β-catenin pathway (Table 1), consistent with the activation of this pathway by the sustained GSK-3 inhibition of Ro3303544. As an example, real-time polymerase chain reaction (qPCR) confirmed the upregulation of *Axin2* (Fig 7C). Considering that the prolonged administration of Ro3303544 drastically affected cell spreading and morphology (Fig 2C), genes related to cell adhesion were then focused on. Integrins are prototypical adhesion receptors that link the extracellular matrix (ECM) to the intracellular actin cytoskeleton. They are heterodimers consisting of an α- and a β-subunit. Within the integrin family, Ro3303544 led to downregulation of the genes for α1, α3, α6, β5, and β1-like integrins, and no member of this family was upregulated (Table 1). Moreover, the expression levels of three genes previously reported to modulate β1-integrin maturation were significantly affected: *N*-acylsphingosine amidohydrolase 3-like (*Asah3l*, also named Acer2; 4.01-fold increase), talin2 (*Tln2*; 52% decrease) and low-density lipoprotein-related protein 1B (*Lrp1b*; 72% decrease).

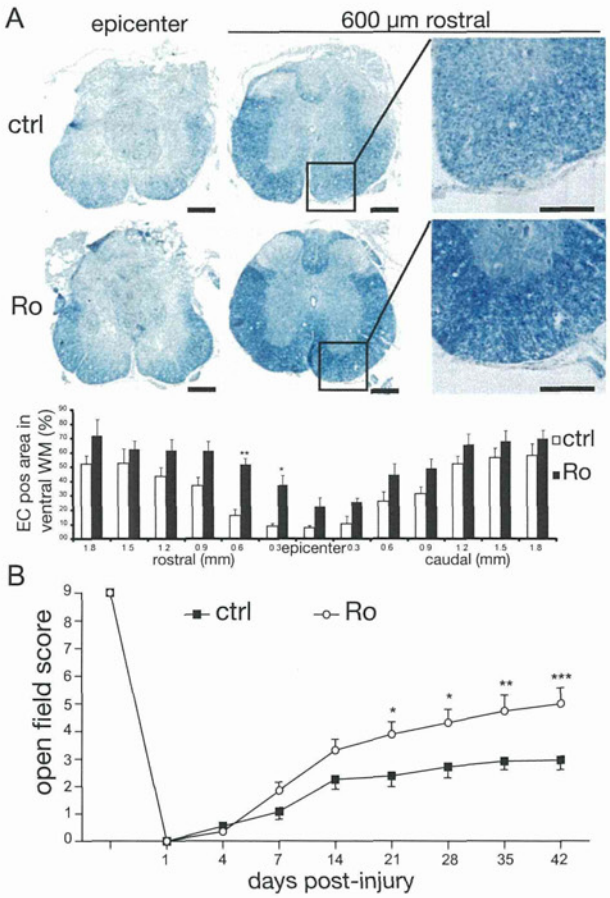

Figure 6. Administration of Ro3303544 reduces demyelination and promotes functional recovery after contusive SCI.

A. Quantitative analysis of eriochrome cyanine-positive areas in the ventral white matter at 42 DPI revealed that treatment with Ro3303544 reduced injury-associated demyelination. Data represent mean ± SEM ($^{**}p < 0.01$, $^{*}p < 0.05$, $n = 5$ mice per group). Scale bars: 250 µm.

B. Hindlimb movement evaluated using the Basso mouse scoring scale improved significantly in the Ro3303544 group compared to the control group from 21 DPI. Data represent mean ± SEM. ($^{*}p < 0.05$, $^{**}p < 0.01$, $^{***}p < 0.001$; 2-way repeated measures ANOVA followed by Bonferroni *post hoc* test, $n = 12$ and 13 mice in the control and Ro3303544 groups, respectively.)

The β1-integrin subunit is synthesized as an 87-kDa polypeptide that undergoes glycosylations in the endoplasmic reticulum and Golgi apparatus (Akiyama & Yamada, 1987). Only the most glycosylated form of β1-integrin, with a mass of ~130 kDa, is found at the cell surface and functions in cell adhesion or cell signalling, justifying its denomination as the mature form. Importantly, the changes observed in *Asah3l*, *Tln2* and *Lrp1b* suggested that Ro3303544 could cause the reduced maturation of β1-integrin. Asah3l overexpression is indeed known to inhibit β1-integrin maturation and thereby reduce cell adhesion to fibronectin or collagen (Sun et al, 2009). Furthermore, downregulation of *Tln2* and *Lrp1b* is known to reduce β1-integrin maturation and cell adhesion (Albiges-Rizo et al, 1995; Salicioni et al, 2004). qPCR confirmed the downregulation of both *Tln2* and *Lrp1b* after Ro3303544 administration (Fig 7C). Since the β1-integrin subunit is a component of most integrin receptors expressed by astrocytes (Takada et al, 2007), the role of this specific subunit was focused on next.

In vitro pro-migratory effect of Ro3303544 relies on decreased cell adhesion strength through a reduced surface expression of β1-integrin

Ro3303544 induced similar pro-migratory effects in astrocytes seeded on transwell membranes coated with laminin or fibronectin (Fig 8A), which are both ligands for β1-integrin-containing heterodimers. By contrast, sustained treatment with Ro3303544 did not stimulate astrocyte migration in the absence of any coating, indicating that the pro-migratory effect of Ro3303544 did not result from a switch to an adhesion-independent migration mode.

Immunoblot analysis of total protein lysates prepared from astrocytes treated for 48 h with various concentrations of Ro3303544 revealed a dose-dependent decrease in the expression level of the ~130-kDa mature β1-integrin (Fig 8B). The intensity of the ~110-kDa band, corresponding to the precursor form of β1-integrin, was inversely correlated with that of the mature form, suggesting that the process of maturation through glycosylation was indeed inhibited by Ro3303544. Flow cytometry confirmed that the reduction in the ~130-kDa mature form of β1-integrin seen with immunoblotting corresponded to reduced cell-surface expression (Fig 8C). Furthermore, the wash-out procedure partially reversed this reduction of cell-surface β1-integrin, consistent with its involvement in the effect of Ro3303544. Complete abrogation of astrocyte migration by a function-blocking monoclonal antibody against β1-integrin demonstrated that this subunit is necessary for the migration of astrocytes under the conditions in which Ro3303544 exerts its pro-migratory effect (Fig 8D).

In integrin-dependent two-dimensional migration models, the highest migration speeds result from an intermediate level of cell–substratum adhesion strength (net adhesion), which allows both rapid focal contact formation and the generation of traction forces (DiMilla et al, 1991). At low net adhesion, migration rates are indeed impaired because the reduced binding strength lowers the force generated at the leading edge (Gaudet et al, 2003; Palecek et al, 1997). Conversely, high net adhesion slows cells down and favours cell immobilization through delayed rear-process retraction. Three factors define net adhesion: substrate ligand level, integrin expression level, and the integrin–ligand binding affinity.

Reduced expression levels of integrins provide a pro-migratory advantage at high ECM protein concentrations (Palecek et al, 1997). Therefore, the effect of Ro3303544 on migration was examined with increasing concentrations of laminin (Fig 8E). At 2 µg/ml laminin, significantly more control than Ro3303544-treated astrocytes migrated. Although this observation may seem to contradict our initial observation of a Ro3303544 pro-migratory effect at 10 µg/ml ECM coating, it is in good agreement with the model: at above 5 µg/ml laminin,

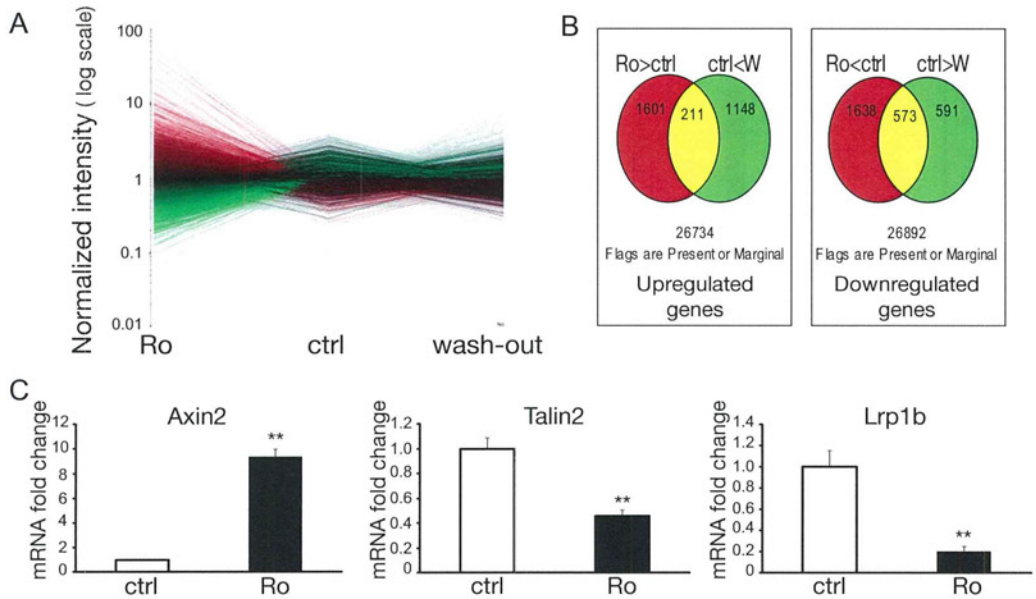

Figure 7. Gene microarray analysis examining the effects of sustained GSK-3 inhibition by Ro3303544 on primary astrocyte cultures.

A. Treatment for 48 h with 1 μM Ro3303544 resulted in a drastic change in the gene expression pattern that could be partially reversed by a 48-h wash-out, $n = 2$ per group. Red: upregulated genes; green: downregulated genes.

B. Diagram illustrating the overlap in genes that were upregulated (left) or downregulated (right) more than twofold in the Ro3303544-treated (Ro: red) and -wash-out (W: green) groups compared to control astrocytes.

C. Significant changes in *Axin2*, *Tln2* and *Lrp1b* mRNA levels detected by qPCR confirmed activation of the Wnt/β-catenin pathway in astrocytes upon prolonged treatment with Ro3303544, as well as the variations in molecules known to modulate β1-integrin signalling. Data represent mean ± SEM. $^{**}p < 0.01$, $n = 5$ (Mann–Whitney test).

treatment with Ro3303544 provided a significant migratory advantage, consistent with the reduced cell-surface expression of β1-integrin in Ro3303544-treated cells. Together, these results suggest that the *in vitro* pro-migratory effect of Ro3303544 relies on decreased adhesion strength, especially through the reduced surface expression of β1-integrin.

Decreased expression of β1-integrin upon Ro3303544 treatment enhances the migration of reactive astrocytes *in vivo*

Since our proposed mechanism for the enhanced migration of astrocytes upon Ro3303544 administration implies the presence of high ECM concentrations, the changes in laminin expression,

Table 1. Gene expression differences of selected gene clusters

Cluster	Abbrev	Accession #	Fold change	Control significance	Ro3303544 significance
Wnt/β-catenin pathway	Apcdd1	AB023957	52.49	P	P
	Wif1	NM_011915	41.02	P	P
	Axin2	NM_015732	20.14	P	P
	Ctnnal1	NM_018761	0.48	P	P
	Wisp2	NM_016873	0.32	P	P
Integrins	Itga3	NM_013565	0.48	P	P
	Itgb5	NM_010580	0.45	P	P
	Itga6	BC024571	0.44	P	P
	Itga6	NM_008397	0.42	P	P
	Itga6	AK045391	0.42	P	P
	Itgbl1	NM_145467	0.42	P	P
	Itga1	AK053377	0.41	P	P
	Itga1	AK053377	0.39	P	P
reported to modulate β1-integrin	Asah3l	NM_139306	4.01	A	P
	Tln2	XM_486227	0.48	P	P
	Lrp1b	BC064765	0.28	P	P, A

P, present; A, absent; ($n = 2$ per group)

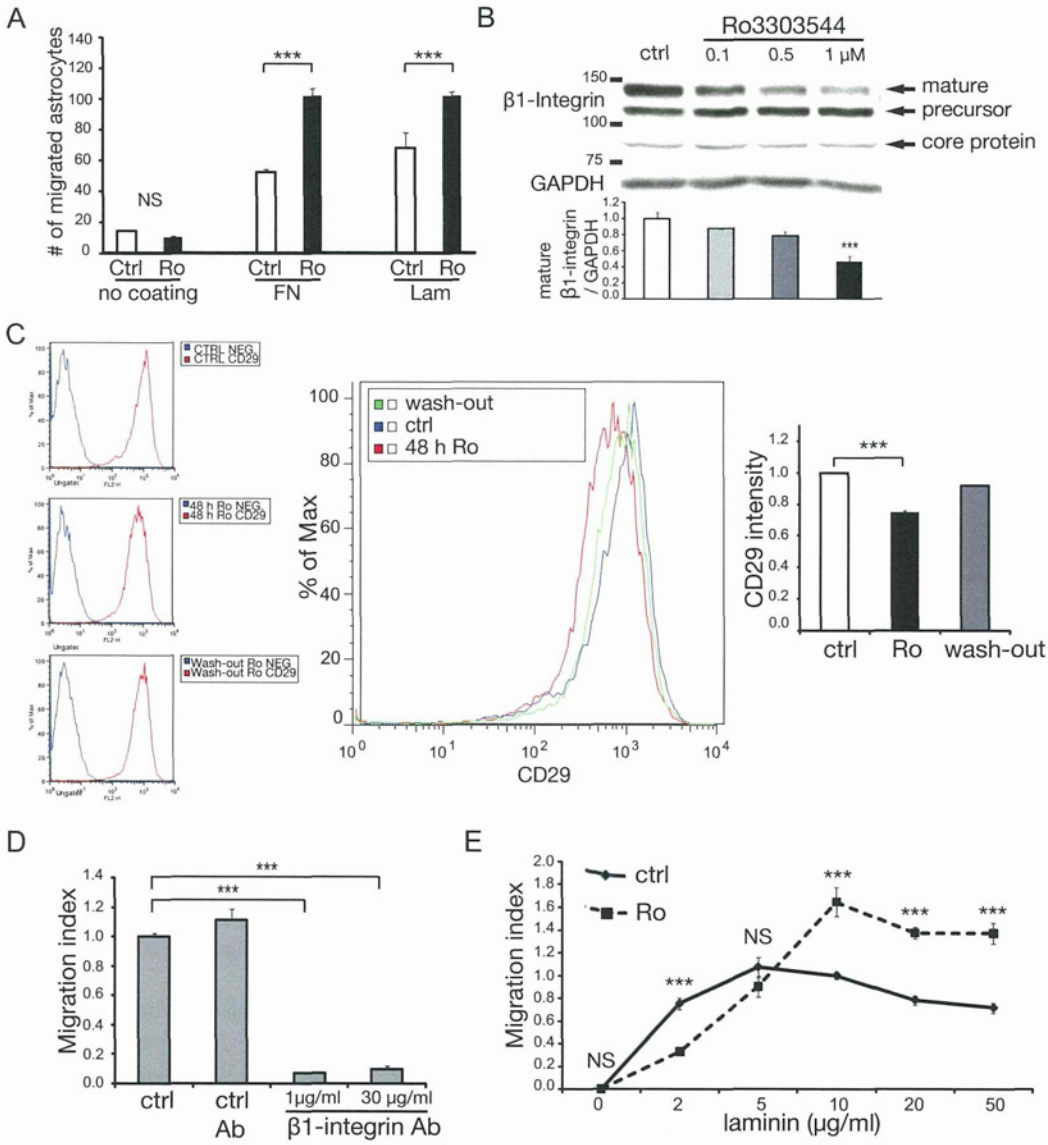

Figure 8. Increased migration of astrocytes *in vitro* upon prolonged Ro3303544 treatment relies on reduced cell adhesion with the ECM due to decreased surface expression of β1-integrin.

A. The pro-migratory effect of prolonged Ro3303544 treatment was similar on fibronectin and laminin. By contrast, migration of astrocytes in the absence of ECM coating was limited regardless of Ro3303544 treatment.

B. Treatment for 48 h with Ro3303544 dose-dependently decreased the expression level of mature β1-integrin in astrocytes. Histogram data represent mean ± SEM of a representative experiment performed in triplicate. $^{***}p < 0.001$.

C. Flow cytometric analysis confirmed that 48-h treatment with Ro3303544 decreased the cell-surface expression of β1-integrin on astrocytes. The specificity of the immunostaining is shown at left. CD29 = β1-integrin. A representative experiment is shown. $^{***}p < 0.001$, $n = 10\,000$ cells per sample (unpaired Student's *t*-test).

D. Migration assays using a function-blocking antibody against β1-integrin demonstrated that functional β1-integrin was required for the migration of the astrocytes.

E. The effect of Ro3303544 on *in vitro* astrocytes migration depended on the ECM concentration. While 48-h treatment with Ro3303544 resulted in decreased migration compared to control cells at low laminin concentrations, a pro-migratory effect was observed at higher concentrations. Data represent mean ± SD of three independent experiments. $^{***}p < 0.001$, $n = 9$.

as an example ECM protein, were examined following SCI. In control animals, while the expression of laminin was initially restricted to blood vessels at 4 and 7 DPI, its expression at the lesion epicentre was drastically upregulated from 10 DPI and maintained at 14 DPI (Fig 9A). The time course of laminin upregulation following injury was not affected by Ro3303544 treatment (not shown). Then, the effect of Ro3303544 administration on β1-integrin expression levels was evaluated *in vivo*. Although the pattern of the different forms of β1-integrin in spinal cord lysates was much more complex than in astrocytes *in vitro*, a significant decrease in the expression level of the higher molecular-weight β1-integrin band in the Ro3303544-treated mice was observed at 5 DPI (Fig 9B). Considering that laminin was upregulated only from 10 DPI, the expression level of β1-integrin was next examined at this time-point. The results showed β1-integrin remain significantly reduced in Ro3303544-treated mice at 10 DPI (Fig 9B).

Together, the observed Ro3303544-mediated reduction in β1-integrin expression in the spinal cord and the concomitant spontaneous upregulation of laminin at 10 DPI suggests that the mechanistic model proposed on the basis of the *in vitro* data is relevant *in vivo*.

DISCUSSION

While the deleterious effects of reactive astrocytes and their associated glial scar after CNS injury are well established (Sofroniew, 2009), their beneficial roles have only been evidenced relatively recently (White & Jakeman, 2008). Using several conditional knock-out mice targeting STAT3 signalling in reactive astrocytes, we and others have previously observed that the compaction of inflammatory cells by migrating reactive astrocytes is associated with enhanced locomotor recovery after SCI (Herrmann et al, 2008; Okada et al, 2006). Here, we report that the pharmacological inhibition of GSK-3 using the novel, highly potent agent Ro3303544 successfully stimulated the migration of astrocytes both *in vitro* and *in vivo* and promoted functional recovery after SCI.

GSK-3 and cell migration

Current data about the role of GSK-3 in cell migration are contradictory (Etienne-Manneville & Hall, 2003; Kapoor et al, 2008). Our observations demonstrate first that the effect of GSK-3 depends on the migration mode involved (interested readers are invited to read the extended discussion in Supporting Information). Although the *in vivo* pattern of endogenous astrocyte migration following CNS injury is unknown, glial cells migrate as single cells during development (Klambt, 2009). Moreover, the observed increased compaction of inflammatory cells *in vivo* after Ro3303544 administration (Fig 4) suggests that the migration of astrocytes observed in the single-cell transwell assay more closely resembles the situation of *in vivo* reactive astrocytes and reveals that the *in vitro* wound scratch assay is not always relevant to *in vivo* CNS injury.

Mechanism of increased migration by the sustained inhibition of GSK-3

The historical model for describing the mesenchymal migration mode (DiMilla et al, 1991; Lauffenburger & Horwitz, 1996; Palecek et al, 1997) implies that cell migration speed depends on the strength of cell adhesion to the substratum. In agreement with the reduced surface expression of β1-integrin, the effect of Ro3303544 on migration was observed to depend on the

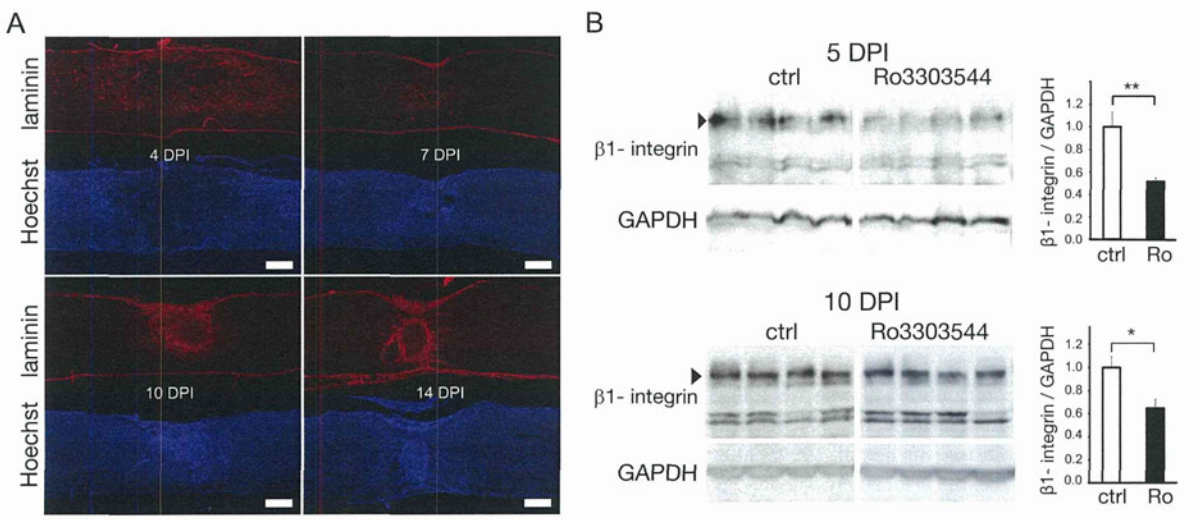

Figure 9. The Ro3303544-mediated reduction of β1-integrin expression in the spinal cord is concomitant with the spontaneous upregulation of laminin at 10 DPI.

A. Laminin was upregulated at 10 DPI in the lesion centre of the injured spinal cord. Red: laminin; blue: Hoechst nuclear staining. Scale bars, 500 μm.

B. At both 5 and 10 DPI, the higher-molecular-weight form of β1-integrin (arrowhead) was significantly decreased in the spinal cord of Ro3303544-treated mice compared to control mice. Data represent mean ± SEM. ($^{**}p < 0.01$, $^{*}p < 0.05$, unpaired t test, $n = 4$ mice per group and time-point.)

concentration of the laminin coating. The apparent discrepancy between the administration period of Ro3303544 *in vivo* (the first 5 days after injury) and the observation that the compaction of inflammatory cells increased compared to control at 14, but not 7 DPI suggests that the pro-migratory effect of Ro3303544 *in vivo* indeed depends on the spontaneous upregulation of ECM proteins following SCI, which we have demonstrated occurs at 10 DPI. Given the complexity of the lesion environment, as well as the number of molecules that potentially modulate the migration of reactive astrocytes, it seems plausible that the actual mechanism for the *in vivo* enhancement of migration by Ro3303544 is more complex than our proposed model.

Mechanism of improved functional outcome by GSK-3 inhibition

The beneficial effect of GSK-3 inhibition in SCI using less potent and specific reagents has been previously reported (Cuzzocrea et al, 2006; Dill et al, 2008). This effect may involve reduced apoptosis and the direct promotion of axon outgrowth. While the direct stimulation of axon growth upon GSK-3 inhibition is still a matter of controversy in the literature (Alabed et al, 2010), we observed that Ro3303544 promoted the neurite outgrowth of embryonic hippocampal neurons *in vitro*, thereby demonstrating its lack of toxicity. However, to selectively evaluate the effects of enhanced astrocyte migration *in vivo*, Ro3303544 administration was restricted to the first 5 days after injury. This protocol allowed us to distinguish the observed results from possible direct axon growth-promoting effects of the drug, because axonal growth is a delayed event.

The observed decrease of astrocyte-devoid spaces filled with CD11b-positive inflammatory cells and the consistent reduction in CSPG- (Fitch & Silver, 1997) and collagen IV-positive areas demonstrated that GSK-3 inhibition at the acute phase of SCI accelerated the compaction of the lesion. We propose that this progressive seclusion of inflammatory cells by reactive astrocytes significantly contributes to the beneficial effect of GSK-3 inhibition after SCI. Although the local inflammatory reaction triggered by SCI is known to be capable of enhancing repair, the involvement of inflammatory cells in secondary neuronal damage such as demyelination is uncontested (Alexander & Popovich, 2009). The beneficial effect of walling off inflammatory cells by scar-forming reactive astrocytes is well established in innate (Bush et al, 1999; Faulkner et al, 2004; Herrmann et al, 2008; Myer et al, 2006; Okada et al, 2006) and adaptive inflammation (Voskuhl et al, 2009).

The major defects observed after ganciclovir-targeted death revealed the contribution of the dividing reactive astrocyte pool to the process of walling off leukocytes after brain and spinal cord injuries (Bush et al, 1999; Faulkner et al, 2004; Myer et al, 2006; Voskuhl et al, 2009). The mitogenic effect of Ro3303544 observed *in vivo* in brain progenitors (Adachi et al, 2007) and *in vitro* in astrocytes led us to investigate whether proliferation was involved in its *in vivo* effect. *In vivo* BrdU incorporation experiments suggest that the contribution of proliferation to the effect of Ro3303544 *in vivo* is not significant.

What is the mechanism whereby the accelerated compaction of inflammatory cells improves functional recovery? Although lesions ultimately demonstrated similar compaction levels at the last time-point examined (42 DPI), locomotor function was permanently superior in the Ro3303544 group compared to control. This observation highlights the critical role of this sub-acute period after the lesion in the recovery process, as previously suggested (Okada et al, 2006). The finding also strongly suggests that white matter sparing is crucial to recovery, as we and others have previously observed when reactive astrocytes wall off inflammatory cells (Faulkner et al, 2004; Herrmann et al, 2008; Okada et al, 2006). Whether remyelination also contributes to the increased myelin staining is difficult to analyse experimentally, as is the conflicting literature concerning the role of β-catenin signalling in remyelination (Azim & Butt, 2011; Fancy et al, 2009).

Given the wide actions of GSK-3 and Wnt/β-catenin, and the role of GSK-3 in inflammation (Jope et al, 2007), additional direct effects of Ro3303544 on inflammatory or immune cells are likely. Nevertheless, the normal infiltration of CD11b cells observed at 7 DPI, the peak of their invasion (Beck et al, 2010), suggests that Ro3303544 does not affect the recruitment of inflammatory cells.

A major question arising from this study is whether our current observation is relevant to other animal models or human SCI. In rat and human, cystic cavity formation is a common complication of brain and spinal cord damage. Unfortunately, these cystic cavities are not observed in most mouse strains, including the C57 BL6/J mice used for this study. *In vitro* studies have suggested that the development of these cavities is closely related to the relationship between inflammatory cells and reactive astrocytes (Fitch et al, 1999). While it is speculated that the physical contraction of the fibrous scar may also contribute to cavity formation in some previous reports (Klapka & Muller, 2006), two recent studies using different experimental approaches have observed that reduction of the scarring was associated with reduced cystic cavities in rat (Iannotti et al, 2006; Xia et al, 2008). However, further studies in relevant models are needed to examine whether the stimulation of reactive astrocyte migration through GSK-3 inhibition does indeed limit the development of these cystic cavities.

In conclusion, our findings reveal a novel beneficial effect of GSK-3 inhibition for SCI and suggest that the pharmacological stimulation of reactive astrocyte migration holds promise as a new therapeutic strategy for the treatment of SCI.

MATERIALS AND METHODS

Antibodies and reagents

The antibodies used are listed in Supporting Information. Ro3303544 was developed by Roche and kindly provided by Dr Gary Pelz (Department of Genetics and Genomics, Roche, Palo Alto, California, USA). The initial characterization of Ro3303544 has been reported elsewhere (Adachi et al, 2007). All the experiments reported in

The paper explained

PROBLEM:

Scarring is a general tissue response after injury to promote wound healing and to separate the injured tissue from the external environment. During the sub-acute phase of contusive SCI, reactive astrocytes migrate to the lesion epicentre and seclude infiltrating inflammatory cells there. This process has been shown to promote functional recovery using several strains of genetically modified mice and models of both innate and adaptive immunity. It is not yet known whether this property of astrocytes can be exploited to aid in the development of better treatment strategies for brain and spinal cord trauma.

RESULTS:

Taking advantage of a novel, highly potent specific inhibitor of GSK-3, Ro3303544, the authors show that inhibition of GSK-3 stimulates astrocyte migration by regulating the expression of β1-integrin both *in vitro* and *in vivo*. Administration of Ro3303544 for the first 5 days after contusive SCI resulted in faster migration of reactive astrocytes, preservation of more myelinated fibres, and significantly improved recovery of movement. Labelling for CSPG and collagen IV confirmed that Ro3303544 treatment reduced the size of the lesion scar.

IMPACT:

Here, for the first time, the authors were able to pharmacologically stimulate the beneficial effect of reactive astrocytes on immune cell restriction and scar formation. These findings reveal a novel effect of GSK-3 inhibition that could improve recovery from SCI and suggest that the pharmacological stimulation of reactive astrocyte migration holds promise as a new therapeutic strategy for the treatment of SCI.

this study compared the effect of Ro3303544 dissolved in DMSO to a control solution that included an equivalent concentration of DMSO (0.1%). BQ-123, BQ-788 and SB415286 were from Sigma.

Cell culture

See Supporting Information for detailed cell culture methods. Briefly, astrocytes in primary cultures were prepared as previously described (Araujo et al, 1993) from 1-day postnatal wild-type C57BL/6J mice.

Modified Boyden's chamber assay (transwell assay)

Polyethelene terephthalate (PET) filters with 8-μm pores (BD Biocoat), used to separate the upper and lower chambers, were coated with 10 μg/ml fibronectin (Sigma) or various concentrations of laminin for 3 h at 37°C. Astrocytes were trypsinized on day 13 *in vitro*, stained with trypan blue, and counted using a hemocytometre. A total of 3×10^4 cells were resuspended in MEM-F12 complete medium containing 1% FBS, 10 μg/ml aphidicolin (Sigma), and the indicated Ro3303544 concentrations, and the cells were allowed to migrate towards the same culture medium supplemented with 10% FBS in the lower chamber. After 15 h at 37°C, the filters were fixed for 20 min at room temperature with 4% paraformaldehyde in PBS (pH 7.5), and the non-migrated cells were removed by wiping the upper side of the membranes with cotton swabs. Cell nuclei were stained using Hoechst 33258, and the filters were mounted on slides in Fluoromount medium (Diagnostic Biosystems). Using Axiovision® software connected to an epifluorescence microscope (Zeiss, Axioplan 2), 12 fields per membrane were captured, and the cells were counted manually.

SCI model

All surgical and animal-care procedures were in accordance with the Laboratory Animal Welfare Act, the Guide for the Care and Use of Laboratory Animals (National Institutes of Health, USA), and the Guidelines and Policies for Animal Surgery provided by the Animal Study Committee of Murayama Medical Center, and they were approved by the ethics committee of Murayama Medical Center. Adult female C57BL/6J mice (8 weeks of age) were anesthetized with an intraperitoneal injection of ketamine (100 mg/kg) and xylazine (10 mg/kg). The dorsal surface of the dura mater was exposed through a laminectomy at the 10th thoracic vertebra, and SCI was induced using an Infinite Horizon impactor (60 kDyn; Precision Systems & Instrumentation, Lexington KY) as previously described (Scheff et al, 2003). Actual impact forces did not differ between groups (control, 62.83 ± 2.55 kDyn; Ro3303544, 62.61 ± 1.98 kDyn). The mice were injected intraperitoneally with 0.5 ml Ro3303544 at 500 μM, dissolved in saline or saline containing an equivalent concentration of DMSO (0.1%) twice daily for 5 days, beginning immediately after SCI. The mice were returned to their cages and given free access to water and food.

Behavioural analysis

Hindlimb motor function was evaluated 1, 3, 7, 14, 21, 28, 35 and 42 days after the injury using the locomotor rating of the BMS (Basso et al, 2006). A team of three experienced examiners evaluated each animal for 4 min and assigned an operationally defined score for each hindlimb, which were then averaged. Animals with incomplete paralysis at 1 DPI (BMS score not equal to zero) were excluded from the study. Data were analysed with two-way repeated measures ANOVA followed by Bonferroni post-hoc test ($n = 12$ and 13 mice in the control and Ro3303544 groups, respectively).

Immunohistochemistry

Techniques and protocols for immunohistochemistry-based analyses are detailed in Supporting Information.

Gene microarray analysis

Microarray processing was performed by the Core Instrumentation Facility of Keio University School of Medicine. Detailed procedures are described in Supporting Information. The data set has been deposited

